Cancer Letters 636 (2026) 218105

Contents lists available at ScienceDirect

Cancer Letters

journal homepage: www.elsevier.com/locate/canlet

Original Articles

Neutrophils exposed to a cholesterol metabolite secrete extracellular vesicles that promote epithelial-mesenchymal transition and stemness in breast cancer cells

Natalia Krawczynska [a,b,*], Yu Wang [a], Ki Lim [a], Anasuya Das Gupta [a], Ralph John Emerson J. Molino [j], Adam Lenczowski [a], Marwan Abughazaleh [a], Shruti V. Bendre [a], Yifan Fei [a], Hannah Kim [a], Lara I. Kockaya [a], Claire P. Schane [a], Dhanya Pradeep [a], Desirée Rodriguez-Casiano [a], Alvaro G. Hernandez [c], Jenny Drnevich [c], Jefferson Chan [b,d,e], Lawrence W. Dobrucki [b,e,f,g], Marni D. Boppart [b,h,i], Stephanie M. Cologna [j], Julie Ostrander [k,l], Erik R. Nelson [a,b,e,m,n,**]

[a] Department of Molecular and Integrative Physiology, University of Illinois at Urbana-Champaign, Urbana, IL, 61801, USA
[b] Beckman Institute for Advanced Science and Technology, University of Illinois at Urbana-Champaign, Urbana, IL, 61801, USA
[c] Roy J. Carver Biotechnology Center, The University of Illinois at Urbana-Champaign, Urbana, IL, 61801, USA
[d] Department of Chemistry, University of Illinois at Urbana-Champaign, Urbana, IL, 61801, USA
[e] Cancer Center at Illinois, University of Illinois Urbana-Champaign, Urbana, IL, 61801, USA
[f] Department of Bioengineering, University of Illinois at Urbana-Champaign, Urbana, IL, 61801, USA
[g] Carle-Illinois College of Medicine, University of Illinois at Urbana-Champaign, Urbana, IL, 61801, USA
[h] Department of Health and Kinesiology, University of Illinois Urbana-Champaign, Urbana, IL, 61801, USA
[i] Carl R. Woese Institute for Genomic Biology- Regenerative Biology & Tissue Engineering, University of Illinois at Urbana-Champaign, Urbana, IL, 61801, USA
[j] Department of Chemistry, University of Illinois at Chicago, Chicago, IL, 60608, USA
[k] Masonic Cancer Center, University of Minnesota, Minneapolis, MN, 55455, USA
[l] Department of Medicine (Division of Hematology, Oncology, and Transplantation), University of Minnesota, Minneapolis, MN, 55455, USA
[m] Carl R. Woese Institute for Genomic Biology- Anticancer Discovery from Pets to People, University of Illinois at Urbana-Champaign, Urbana, IL, 61801, USA
[n] Division of Nutritional Sciences, University of Illinois Urbana-Champaign, University of Illinois at Urbana-Champaign, Urbana, IL, 61801, USA

ARTICLE INFO

Keywords:
27-Hydroxycholesterol
Extracellular vesicle
Neutrophil
Breast cancer
EMT
Stemness

ABSTRACT

Breast cancer is very prevalent. Although detection and treatment of primary disease has improved significantly, 20–30 % of patients will develop recurrent metastatic disease; this stage being associated with poor survival. Small extracellular vesicles (sEVs) are emerging as critical mediators of intercellular communication in the tumor microenvironment (TME). Here, we investigate the mechanisms by which sEVs derived from neutrophils treated with the cholesterol metabolite, 27-hydroxycholesterol (27HC), influence breast cancer progression. Interestingly, sEVs released from 27HC treated neutrophils enhanced epithelial-mesenchymal transition (EMT) and stem-like properties in breast cancer cells. This resulted in a striking loss of adherence, increased migratory capacity and resistance to cytotoxic chemotherapy. When exploring the potential mechanism, we found that EVs from 27HC-treated neutrophils had altered microRNAs (miR) expression. Decreased miRs within 27HC-sEVs, particularly of the let-7 family, resulted in activation of the WNT/β-catenin signaling pathway in recipient cancer cells, suggesting that this may be a predominant pathway for adopting stem-like properties. Our findings underscore a novel mechanism by which a cholesterol metabolite can modulate neutrophils and thereby contribute to breast cancer pathophysiology through EV-mediated intercellular communication. This work represents the first steps in developing this axis for potential therapeutic interventions.

* Corresponding author. Department of Molecular and Integrative Physiology, University of Illinois at Urbana-Champaign, Urbana, IL, 61801, USA.
** Corresponding author. Department of Molecular and Integrative Physiology, University of Illinois at Urbana-Champaign, Urbana, IL, 61801, USA.
E-mail addresses: nataliak@illinois.edu (N. Krawczynska), enels@illinois.edu (E.R. Nelson).

https://doi.org/10.1016/j.canlet.2025.218105
Received 8 June 2025; Received in revised form 28 September 2025; Accepted 27 October 2025
Available online 28 October 2025

1. Introduction

Despite significant advances in diagnosis and treatment, metastatic disease accounts for more than 90 % of breast cancer-related deaths. Breast cancer is the most diagnosed cancer and the leading cause of cancer-related death in women world-wide [1,2]. Triple-negative breast cancer (TNBC) accounts for approximately 15–20 % of breast cancer cases [3] and 10–20 % of invasive breast cancers [4]. TNBC is defined as a type of breast cancer with negative expression of estrogen (ER), progesterone (PR), and human epidermal growth factor receptor-2 (HER2), and thus is not sensitive to endocrine therapy. Therefore, with the exception of BRCA pathogenic variant carriers or the use of immune checkpoint blockers in the adjuvant setting, surgery followed by combined chemotherapy and radiation interventions are the main treatments for this type of breast cancer [5–9]. For those reasons, identifying new therapeutic targets for the successful treatment of metastatic breast cancer, especially for the TNBC subtype, is urgent.

Cholesterol is essential for maintaining the normal function of cells; it influences cell membrane integrity and lipid metabolism [10]. Cholesterol can be supplemented from the diet or synthesized *de novo*. It is catabolized through two major bile acid synthesis pathways initiated by the rate limiting enzymes CYP7A1 and CYP27A1, respectively [11]. As it is metabolized into bile acids, several oxysterol intermediates are formed [12]. 27-hydroxycholesterol (27HC) is the most abundant oxysterol in human circulation [13,14] and works as a selective estrogen receptor modulator (SERM) and liver X receptor modulator (SLXRM) [15–17]. Both cholesterol and 27HC play important roles in regulating cellular function [17–19].

Whether cholesterol is associated with the risk of a primary diagnosis of breast cancer is unclear [12]. A large meta-analysis of breast cancer patients found no association between the use of statins (one type of cholesterol lowering medication) and breast cancer onset [20]. Caveats to approaches and our interpretations of these data such as not considering body-mass-index, menopausal status etc. have been reviewed [12,21]. However, elevated cholesterol concentrations are associated with breast cancer recurrence [22]. Several studies report associations between statin use and either recurrence, poor prognosis or survival for breast cancer patients, including for those of the triple negative subtype [23–28]. Use of statins during adjuvant endocrine therapy is correlated with improved disease free survival and distant recurrence free survival [29]. Thus, while cholesterol may not be carcinogenic in and of itself, it is clearly associated with progression.

Whether circulating concentrations of 27HC is a risk or prognostic factor is also not clear, but likely depends on breast tumor subtype, menopausal status, circulating estradiol, and racial and ethnic group [13,30–32]. Since CYP27A1, the enzyme that synthesizes 27HC, is highly expressed in myeloid immune cells, circulating 27HC may not be reflective of local concentrations within the tumor, and so circulating concentrations of 27HC may have little prognostic value. Indeed, in preclinical models, the genetic deletion of CYP27A1 only in myeloid immune cells was sufficient to impair tumor growth and metastasis of mammary and ovarian tumors [33,34]. Breast tumors have higher 27HC concentrations compared to adjacent normal and healthy breast tissue [18]. In addition, higher mRNA expression of the enzyme responsible for the catabolism of 27HC, CYP7B1 has been associated with better overall patient survival rates in breast cancer patients [35].

Mechanistically, 27HC works through two major nuclear receptors: the liver X receptors (LXRs) and estrogen receptors (ERs). Several oxysterols such as 27HC activate the LXRs which coordinate a genetic program to increase cholesterol efflux and decrease cholesterol synthesis. As such, LXRs tend to be anti-proliferative for cancer cells, which require abundant cholesterol supplies for division [33,36]. However, in models of ERα+ breast or endometrial cancer, the stimulatory activities of 27HC through ERα receptor appear to outweigh those of LXR, resulting in increased proliferation and tumor growth [15,17,18].

In addition to its cancer cell-intrinsic effects, 27HC has been found to robustly increase metastasis in murine models of mammary cancer, in a manner requiring myeloid immune cells [34,37]. At each step of cancer development, from initiation through promotion and metastatic progression, cancer cells have to escape from immune surveillance to survive in the host system [38]. 27HC works through the LXR to shift myeloid immune cells, including neutrophils, into an immune-suppressive phenotype, impairing T cell expansion and function [33,34,39]. For mammary metastasis to the lung in mice, the neutrophil myeloid cell type ($CD11B^{+}$;$Ly6G^{+}$ cells) was found to mediate the pro-metastatic effects of 27HC [37].

Although they are the most abundant leukocytes in the blood, neutrophils have been underappreciated in cancer development. However, in the last decade, several seminal studies have implicated neutrophils in breast cancer progression and metastasis [40–48]. Neutrophils can infiltrate both the tumor microenvironment (TME) and pre-metastatic niche [49,50]. Due to their plasticity and heterogeneity, neutrophils have been reported to be anti-tumor and pro-tumor immune cells [49,51,52]. Interestingly, treatment with exogenous 27HC was found to increase the number of neutrophils within tumors and metastatic lesions of preclinical murine models of mammary cancer [19]. Subsequent work found that 27HC shifts myeloid cells, such as neutrophils, into a highly immune-suppressive phenotype by modulating the activity of the LXR [33,34,39].

While investigating the mechanisms by which 27HC regulates neutrophils and metastasis, we found that 27HC increased the secretion of small extracellular vesicles (sEVs, including exosomes) from neutrophils [53,54]. sEVs from neutrophils treated with 27HC stimulated tumor growth and metastasis in murine models of TNBC [53]. However, it is not known how these 27HC-derived sEVs stimulate metastasis.

sEVs are lipid-bilayer membrane-enclosed vesicles that are heterogeneous in size, 30nm–150nm, and released from all cell types [55]. sEVs serve as a method of intercellular communication between different cell types, transferring a complex mixture of cargo including DNA, RNA, proteins, metabolites, and even mitochondria under some conditions [55,56]. There are a limited number of studies focusing on sEVs from neutrophils in cancer progression [57]. For example, sEVs from neutrophils have been implicated in reprogramming the TME and can promote both tumor progression and regression [58]. They have also been implicated in the metastatic process, mediated via nicotine activation in lung [59] and breast [60] cancers. Thus, how the cargo of sEVs is altered by different conditions and how neutrophil-derived sEVs influence tumor pathophysiology are critical to our understanding of tumor progression, and ultimately developing therapies around them.

Here, we describe our findings that sEVs from 27HC-treated neutrophils led to mammary cancer cells losing their adherent properties. MicroRNAs (miRs) in normal sEVs from neutrophils inhibited the WNT/β-catenin pathway in recipient cancer cells, a regulatory mechanism which was lost in sEVs from 27HC-treated neutrophils. Consequently, cells receiving sEVs from 27HC-treated neutrophils gained a stem-like phenotype and underwent epithelial-mesenchymal transition (EMT), the consequences of which may lead to increased metastasis and drug resistance.

2. Materials & methods

2.1. Reagents

27-hydroxycholesterol (27HC, purity ≥98 %) was synthesized and purchased from Sai Labs or Sigma-Aldrich. Doxorubicin hydrochloride was purchased from MedChemExpress. Antibodies were purchased from BD Pharmingen: CD24 (FITC, Cat:561777), and CD44 (APC, Cat:559250). ALDH1A1 antibody stain was a gift from Professor Jefferson Chan Department of Chemistry, University of Illinois at Urbana-Champaign.

2.1.1. Reagents for LC-MS/MS

27-hydroxycholesterol, 27-hydroxycholesterol d6, 22(R)-hydroxycholesterol, and 22(S)-hydroxycholesterol were purchased from AvantiPolar lipids (Alabaster, AL). 24(R)-hydroxycholesterol, 24(S)-hydroxycholesterol, and 25-hydroxycholesterol were from Cayman Chemicals (Ann Arbor, MI). 4-Dimethylaminophenylisothiocyanate (DMAPI) and sequencing grade dimethylformamide (DMF) came from Thermo Fisher Scientific (Waltham, MA). Triethylamine (HPLC, LiChropur™, ≥99.5 % (GC), used as a catalyst for the derivatization of hydroxycholesterols, together with organic solvents required for lipid extraction (chloroform, methanol, hexane, all LC-MS grade) were supplied by Sigma Aldrich (St. Louis, MO). Formic acid utilized as a solvent additive, and 45 % KOH necessary for the base hydrolysis of esterified hydroxysterols were also from Sigma Aldrich.

2.2. Animals

All protocols involving the use of animals were approved by the University of Illinois Institutional Animal Care and Use Committee (IACUC). Female BALB/c mice between 8 and 10 weeks of age were purchased from Charles River Laboratories and housed at the University of Illinois in individually vented cages at 3 to 5 mice per cage; under specific pathogen-free, temperature- and humidity-controlled conditions, with a 12-h light/12-h dark schedule. Food and water were provided ad libitum.

2.3. Cell culture

4T1 cells were a gift from Mark Dewhirst (Duke University School of Medicine). EMT6 cells were purchased from the American Type Culture Collection (ATCC, USA). MCF7 cells were a gift from Donald McDonnell (Duke University School of Medicine). Medium for cell lines and primary cell culture - RPMI 1640, DMEM, or DMEM F12 were supplemented with 1 % penicillin/streptomycin (Corning), 1 % nonessential amino acid (Corning), 1 % sodium pyruvate (Corning), and 10 % fetal bovine serum (FBS, Gibco). After adding mentioned reagents media was called "complete". In experiments requiring the harvest or usage of EVs, 10 % EV-depleted FBS (Gibco) was added in place of normal serum. Cell lines were free from mycoplasma and routinely tested.

2.4. Cell lines

Murine mammary cancer cell lines – 4T1, EMT6, were grown in Dulbecco's modified Eagle's medium; MCF7 in Dulbecco's modified Eagle's F12 medium supplemented with 1 % nonessential amino acid, 1 % sodium pyruvate, 1 % penicillin/streptomycin, and 10 % fetal bovine serum (FBS). In experiments requiring the harvest or usage of EVs, 10 % EV-depleted FBS was added in place of normal serum.

2.5. Isolation of LY6G cells - neutrophils

Ly6G positive cells were isolated from mice bone marrow using Anti-Ly6G MicroBeads UltraPure (Miltenyi Biotec) according to the protocol. Briefly, femurs and tibia from 8 to 12-week-old WT BALB/c mice were collected and briefly soaked in 70 % ethanol, and rinsed in phosphate-buffered saline (PBS, Lonza). Sterile medium (RPMI) was used to flush bone marrow over a 70-μM filter. Collected cells were used for Ly6G-positive cell isolation according to the protocol. Isolated cells were used immediately for experiments. The purity of neutrophils after isolation was verified to be at least 93 % by flow cytometry for CD11B and Ly6G.

2.6. Extracellular vesicles isolation and characterisation

Extracellular vesicles were isolated from conditioned media after 24 and 48hrs of incubation using a commercially available kit - ExoQuick-TC ULTRA (SBI), according to the manufacturer's protocol. Characterization of isolated sEVs was done as previously described [53]. Briefly, we performed size characterization by Nanoparticle analysis by NanoSight NS300, Malvern Panalytical (see: PARTICLE ANALYSIS), and flow cytometry of known sEVs markers (CD9, CD63, CD81) using Attune Nxt Flow Cytometer and FCS Express 6 Software (see: *FLOW CYTOMETRY)*. sEVs were stored at −80 °C for no longer than 5 days after isolation prior to use.

2.7. Particle analysis

The concentration of sEVs was measured using nanoparticle tracking analysis (NTA; NanoSight NS300, Malvern Panalytical). Three 30 s videos were captured and analyzed for each sample using NTA3.1 software. During capture, screen gain was set at 1.0 and the camera level at 11. For analysis, screen gain was set at 10.0 and detection setting at 5.

2.8. LC-MS/MS of oxysterols

Quantification of oxysterols was performed at two independent sites: Metabolon and The University of Illinois Chicago.

2.8.1. Extraction and derivatization of hydroxycholesterols

Sample treatment combined parts of workflows presented by two previous studies [61,62]. Collected cell culture media and purified EVs were spiked with 5 μg d6 27-hydroxycholesterol internal standard prior to dilution with ultrapure water to a final volume of 1 mL. Then, samples were probe sonicated in a QSonica Q125 probe sonicator three times with 50 % amplitude for 10 s (1 s pulses). After which, lipid extraction was performed through the direct addition of 4 mL 2:1 chloroform/methanol mixture (Folch Method). The organic layers from two successive partitioning were pooled and concentrated in a stream of nitrogen gas. Then, dried material was resuspended in 1M KOH in 60 % ethanol and allowed to saponify overnight under room temperature and minimal shaking. Following the addition of 1 mL water to this aqueous phase, free unesterified hydroxycholesterols were collected through partitioning with 2 mL hexane, a step repeated three more times to maximize recovery. The combined organic layer was dried under a stream of nitrogen prior to derivatization.

Both standard hydroxycholesterols (2.5 pg/μL – 50 ng/μL) and samples were resuspended in 200 μL DMF with 10 mg/mL DMAPI. Derivatization was catalyzed by the addition of 30 μL triethylamine (TEA). Incubation under dark conditions and 200 rpm shaking was done for 2 h under 65 °C. The reaction was immediately quenched with 150 μL phosphate buffer (pH = 8) prior to the extraction of derivatized hydroxycholesterols with 3 mL hexane. After drying under nitrogen gas, standard solutions were resuspended in 10:1 acetonitrile/isopropanol to a final volume of 200 μL. Unknown samples were similarly prepared but diluted with a smaller volume of 25 μL.

2.8.2. Mass spectrometry-based detection of oxysterols

2.8.2.1. Analysis by metabolon. Study samples were analyzed by LC-MS/MS for total cholesterol, lanosterol, 5α,6β-dihydroxycholestanol (5α, 6β-diHOC), 7α,27-dihydroxycholesterol (7α,27-diHOC), 24-hydroxycholesterol (24HOC), 27-hydroxycholesterol (27HOC), 4β-hydroxycholesterol (4βHOC), 5α,6α-epoxycholesterol (5α,6α-epoxy), 7 dehydrocholesterol (7DHC), 8-dehydrocholesterol (8DHC), desmosterol, and lathosterol following Metabolon Method TAM227: "LC-MS/MS Quantitation of Sterols and Oxysterols in Human Plasma". Underivatized Analysis.

For the analysis of total cholesterol, lanosterol, 5α, 6β-diHOC, and 7α,27-diHOC, 50.0 μL of study sample was spiked with internal standard solution, hydrolyzed, and extracted by liquid-liquid extraction with hexane. Following centrifugation, the hexanes layer was evaporated to

dryness, reconstituted in acidified methanol, and injected onto an Agilent 1290/SCIEX 6500+ Triple Quadrupole LC-MS/MS system equipped with an Acquity BEH Shield RP18 Column. The mass spectrometer was operated in positive mode using atmospheric pressure chemical ionization (APCI).

For the analysis of 24HC, 27HC, 4βHOC, 5α,6α-epoxy, 7DHC, 8DHC, desmosterol, and lathosterol, a separate 50.0 μL of study sample was spiked with internal standard solution, hydrolyzed, extracted by liquid-liquid extraction with hexanes, and then derivatized. Following derivatization, a second liquid-liquid extraction with hexanes was performed. Upon centrifugation, the hexanes layer was evaporated to dryness, reconstituted in acidified methanol, and injected onto an Agilent 1290/SCIEX 5500 QTRAP LC-MS/MS system equipped with an Acquity BEH Shield RP18 Column. The mass spectrometer was operated in positive mode using electrospray ionization (ESI).

The peak areas of the respective analyte product ions were measured against the peak areas of the corresponding internal standard product ions. Quantitation was performed using a weighted linear or quadratic (for cholesterol) least squares analysis generated from fortified calibration standards prepared concurrently with study samples. LC-MS/MS raw data were collected using SCIEX software Analyst 1.7.3 and processed using SCIEX OS-MQ v3.1.6.

2.8.2.2. Analysis by University of Illinois Chicago. Chromatographic separation of isomeric hydroxycholesterols was performed in an Agilent 1290 Infinity II ultrahigh performance liquid chromatography system coupled to a 6550 iFunnel quadrupole time-of-flight (qTOF) mass spectrometer also from Agilent. 20 μL of each sample was injected onto an Agilent Poroshell 120 EC-C18 column (2.7 μm, 2.1 × 100 mm), after which, 1 μL of diluted standard solutions immediately followed. Binary mobile phase flowed at 0.4 mL/min and 50 °C. Specifically, aqueous Solvent A is water with 0.1 % formic acid, while Solvent B is 70/30 Acetonitrile with 0.1 % formic acid. Baseline separation of the derivatized hydroxycholesterols was obtained through an elution method with 70 % B beginning from 0 to 1 min, 77 %B at 5 min, 92 % B at 16 min, 100 % B at 17 min, back again to 70 % B at 18 min further held for three more minutes prior to the next injection.

Positive mode electrospray ionization of hydroxycholesterols was carried out using an Agilent Jetstream Source (AJS). The capillary voltage was set at 3.5 kV, nebulizer pressure of 50 psi, gas temp at 200 °C, drying gas 11 L/min, sheath gas temperature of 300 °C, and sheath gas flow of 12 L/min. Focusing only on derivatized hydroxycholesterols, the detection was focused between the *m/z* 350–600 range. Full-scan MS1 spectra were acquired at a rate of 6 spectra per second.

Peak detection and integration necessary for quantification were through batch processing of generated raw (.d) files in the Agilent MassHunter Profinder software. Detector responses for *m/z* 565.4369 and *m/z* 571.4839, corresponding to the $[M+H]^+$ ions of the hydroxycholesterols and the d6-internal standard, correspondingly, were extracted and exported for statistical analysis. Oxysterol identification was validated using both retention time and fragmentation spectra.

2.9. Treatment of neutrophils with Let-7 inhibitors

After isolation, $0.45x10^6$ Ly6G positive cells were seeded in 6-well plates in 1.9 mL RPMI EVs depleted complete media and treated with four let-7 inhibitors or negative control for inhibitor (NC) cocktail (Qiagen miRCURY LNA miRNA inhibitors, a modified antisense). The transfection reaction was constructed according to the manufacturer's protocol. Briefly, for 1 sample we prepared accordingly: 100uL of media, 3uL of HiPerFect transfection reagent (Qiagen), and 1uL of 10uM let-7 inhibitors (inhibitors for let-7a-5p, let-7g-5p, let7f-5p, and let7j) or NC. The final concentration of the inhibitors was 5 nM. The prepared transfection reagent was mixed and incubated at room temperature for 10 min and added drop-wise to the cells. After 48h of culture cells were harvested. Cells were used for RNA and subsequent miR expression analysis as described below (see: *miRs QUANTIFICATION - REAL TIME-QUANTITATIVE POLYMERASE CHAIN REACTION (RT-qPCR)*). Conditioned media were collected for sEVs isolation followed by miRs expression evaluation and cancer cells treatments.

2.10. Cancer cell treatment with small extracellular vesicles

20K of 4T1 and EMT6, and 50K of MCF7 cells were seeded in 12-well plates in 1 mL of "complete" DMEM or DMEM F12 media supplemented with commercially available EV-depleted FBS (Gibco). At the time of seeding, sEVs were added to the cell culture, followed every 24h of treatment. A schematic overview of the experimental design is presented in Fig. 1A.

2.11. Co-treatment of cancer cells with extracellular vesicles and Let-7 MIMCS – rescue experiment

20K EMT6 cells were seeded in 12-well plates in 0.9 mL of "complete" DMEM media supplemented with commercially available EV-depleted FBS (Gibco). At the time of seeding, cells were treated with a cocktail of four let-7 mimics (let-7a-5p, let-7g-5p, let-7f-5p and let-7j) or negative control for mimics (NC) (Qiagen miRCURY LNA miRNA Mimics). The transfection reaction was constructed according to the manufacturer's protocol. Briefly, for 1 sample we prepared: 100uL of media, 3uL of HiPerFect transfection reagent (Qiagen), and 1uL of 10uM let-7 mimics (mimics for let-7a-5p, let-7g-5p, let-7f-5p, and let-7j) or NC. The final concentration of the inhibitors was 10 nM. The prepared transfection reagent was mixed and incubated at room temperature for 10 min and added drop-wise to the cells. After 4h of transfection, sEVs were added to the cell culture, followed every 24h treatment. At the specified time point, cells were collected for gene expression sis using RT-qPCR.

2.12. Small RNA sequencing

2.12.1. Total RNA isolation

Total RNA from Ly6G cells and extracellular vesicles was isolated using miRNeasy Micro kit (Qiagen) according to the manufacturer's protocol with supported modification for small RNA quantities. The quantity and quality of isolated RNA were determined with Qubit Fluorometer (Thermo Fisher Scientific), Bioanalyzer 2100 and Fragment Analyzer (Agilent).

2.12.2. Construction of short RNA (miRNA) libraries

Construction of libraries and sequencing on the Illumina NovaSeq 6000 were performed at the Roy J. Carver Biotechnology Center at the University of Illinois at Urbana-Champaign. Purified total RNAs from DMSO (vehicle) or 27HC treated cells' EVs were converted into miRNA libraries with the QIAseq miRNA library preparation kit (Qiagen). The individually barcoded libraries were quantitated with Qubit (ThermoFisher) and run on a Fragment Analyzer (Agilent) to confirm the presence of a fragment of the expected length. The libraries were pooled in equimolar concentration and further quantified by qPCR on a CFX Connect Real-Time qPCR system (Bio-Rad) for maximization of the number of clusters in the flow cell.

2.12.3. Sequencing of libraries in the NovaSeq

The barcoded miRNA libraries were loaded on a NovaSeq (Illumina) for cluster formation and sequencing. The libraries were sequenced from one end of the fragments for a total of 100 nucleotides. The fastq read files were generated and demultiplexed with the bcl2fastq v2.20 Conversion Software (Illumina). The quality of the demultiplexed fastq files was evaluated with the FastQC software, which generates reports with the quality scores, base composition, k-mer, GC and N contents,

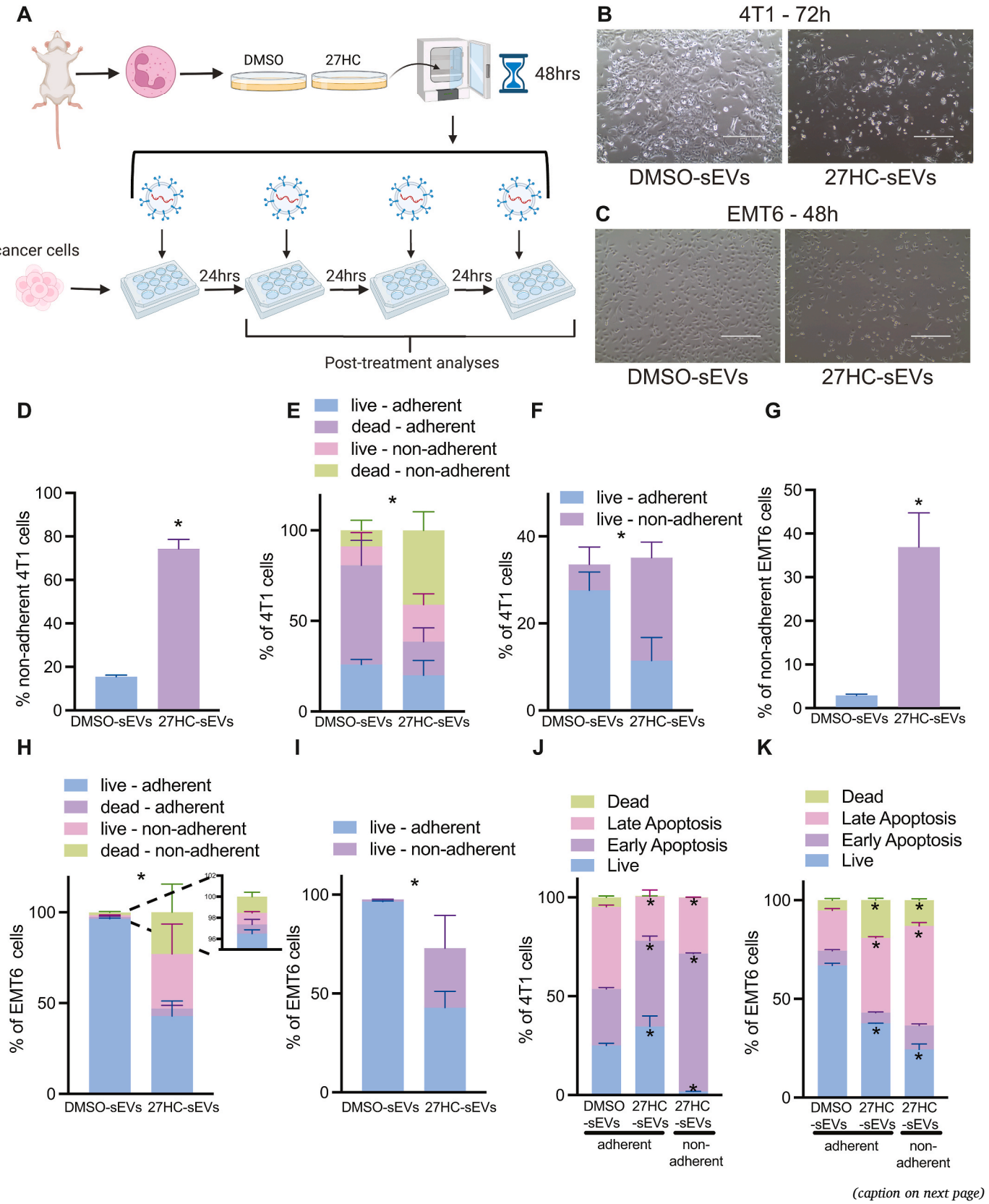

(caption on next page)

Fig. 1. ***sEVs from 27-hydroxycholesterol treated neutrophils promote loss of adherence in breast cancer cells.*** **(A)** A schematic overview of the experimental setup. Neutrophils were isolated from the bone marrow of the tibia and femur of female mice and cultured in EV-depleted media with indicated ligands for 48h. After a designated time, neutrophil-EVs were isolated and resuspended in PBS. Cancer cells were sub-cultured and exposed to daily treatment with neutrophil-EVs. Cancer cells were harvested at specific time points for subsequent analyses. Representative pictures of 4T1 **(B)** and EMT6 **(C)** cancer cells after exposure to DMSO-sEVs or 27HS-sEVs for 72h or 48h, respectively. **(D)** Quantification of non-adherent 4T1 cells after 72h of the treatments. **(E)** Quantification of live and dead cells in the attached and detached subpopulations of 4T1 cells after 72h of the treatments. Trypan blue staining and an automatic cell counter (Countless 3, Invitrogen) were used. **(F)** Quantification of live-adherent and live-non-adherent cells in the attached and detached subpopulation of 4T1 cells after 72h of the treatments. Trypan blue staining and an automatic cell counter (Countless 3, Invitrogen) were used. **(G)** Quantification of non-adherent EMT6 cells after 48h of the treatments. **(H)** Quantification of live and dead cells in the attached and detached subpopulations of EMT6 cells after 48h of the treatments. Trypan blue staining and an automatic cell counter (Countless 3, Invitrogen) were used. **(I)** Quantification of live-adherent and live-non-adherent cells in the attached and detached subpopulations of EMT6 cells after 48h of the treatments. Trypan blue staining and an automatic cell counter (Countless 3, Invitrogen) were used. **(J–K)** Quantification of flow cytometry analysis of 4T1 **(J)** and EMT6 **(K)** cells after 72h and 48h of the treatments, respectively, stained with annexin V and PI for live-dead cells evaluation. Cells were divided into 4 subpopulations: live cell (Annexin V-/PI-), early apoptotic cell (Annexin V+/PI-), late apoptotic cell (Annexin V+/PI+), and dead cell (Annexin V-/PI+). Statistical analyses were performed using: the Student's T test (**D&G**), Fisher exact test (**E-F, H-I**), one-way ANOVA followed by a multiple comparison test with Šidák's correction (**J-K**). N = 3/treatment group. An asterisk (*) denotes statistical significance ($P < 0.05$). All data are presented as mean ± SEM. (For interpretation of the references to color in this figure legend, the reader is referred to the Web version of this article.)

sequence duplication levels and overrepresented sequences.

2.12.4. Alignment and counts

FASTQ read data were processed using the nf-core smrnaseq workflow v1.1.0 [63], using miRBase 22.1 [64] and Gencode M25 [65]. The workflow was run using Nextflow v. 21.10.6 [66] with the command line call 'nextflow run nf-core/smrnaseq -r 1.1.0 -c smrna.conf', with the workflow configuration file settings including the miRNA protocol to 'qiaseq' and the species to 'mmu'.

2.12.5. Statistical analysis of small RNA-seq

The mature counts were read into R (v4.1.2) and normalized using TMM [67]. miRNA genes without at least one count in four samples were removed. Final normalized expression values were made by re-running TMM and then converting to log2-based counts per million (logCPM) using edgeR's cpm function [68]. Differential gene expression (DE) analysis was performed using the limma-trend method using a model of ~Treatment + Group to control for batch effects of the sample processing group. Multiple testing correction was done using the False Discovery Rate method [69]. RNA-Seq data has been submitted to the NCBI Gene Expression Omnibus (accession number: GSE272477).

2.12.6. Downstream analysis of small RNS-seq

Different strategies were employed for downstream analysis. As the first step, we searched for targeted genes by our statistically differently expressed microRNA between DMSO vs. 27HC groups. Briefly, putative targeted genes were predicted by four different databases: TargetScanMouse (TargetScanMouse 7.2), miRDB (miRDB - MicroRNA Target Prediction Database), miRWalk (Home - miRWalk (uni-heidelberg.de)), and miRTarBase (miRTarBase: the experimentally validated microRNA-target interactions database (cuhk.edu.cn)). Only genes that were predicted to be potential targets of our microRNA in three out of four databases were taken under further investigation. In the first strategy, analysis of genes that were targeted by the greatest number of miRs were analyzed. In the second strategy, targeted genes were used for pathway analysis using four different approaches: KEGG (KEGG: Kyoto Encyclopedia of Genes and Genomes), PANTHERDB (pantherdb.org/?msclkid=3e954a57aba411ecb1b9fdc5b826ea61), g:Profiler (g:Profiler – a web server for functional enrichment analysis and conversions of gene lists (ut.ee)), and STRING (STRING: functional protein associations networks (string-db.org)). The third strategy of downstream analysis employed mirPath v.3 software (DIANA TOOLS - mirPath v.3 (uth.gr)) for combined analysis of up and down-regulated microRNAs between tested groups, using microT-CDS (v5.0) as a database for pathway analysis.

2.13. miR Quantification - real time-quantitative polymerase chain reaction (RT-qPCR)

Isolated total RNA from Ly6G cells and extracellular vesicles was used for validation of microRNA sequencing by RT-qPCR according to the manufacturers' protocols. Briefly, 10 ng of isolated total RNA was reverse transcribed into complementary DNA (cDNA) using miRCURY LNA RT Kit (Qiagen). The cDNA was then amplified with specific commercially available primers for selected miRs using miRCURY LNA SYBR Green PCR Kit (Qiagen) using Bio-Rad CFX384 Thermal Cycler (Bio-Rad). In addition to each cDNA synthesis reaction, an UniSp6 RNA was added as an external control and used for data normalization and relative expression analysis via the $2^{-\Delta\Delta CT}$ method.

2.14. Real time-quantitative polymerase chain reaction (RT-qPCR)

GeneJet RNA Purification kit (Thermo Fisher) was used for RNA extraction, according to the manufacturer's protocols. cDNA was synthesized using iScript Reverse Transcription Supermix (Bio-Rad), according to the manufacturer protocols. Primer-BLAST software (https://www.ncbi.nlm.nih.gov/tools/primer-blast/) was used for primer design. A list of all used primers is presented in Supplementary Table 3 mRNA gene expression was quantified using iTaq Universal SYBR Green Supermix (Bio-Rad) on a Bio-Rad CFX384 Thermal Cycler (Bio-Rad). Relative expression was determined via the $2^{-\Delta\Delta CT}$ method and normalized to the housekeeping gene (TATA box binding protein).

2.15. Flow cytometry

For all flow cytometry experiments, samples were analyzed using the Attune Nxt Flow Cytometer and FCS Express 7 Software.

2.15.1. Cell death

For cell death assays, 20×10^5 4T1/EMT6 cells were seeded in 12 well plates and treated for 72/48hrs with sEVs from DMSO/27HC-neutrophils. Cells were harvested and stained using the FITC Annexin V/PI Dead Cell Apoptosis Kit (Invitrogen) following manufacturer protocol. Samples were analyzed and cell status (live, early apoptotic, late apoptotic, or dead) was determined.

2.15.2. EVs markers

To characterize isolated sEVs, we have quantified known EVs markers (CD9, CD63, CD81) using flow cytometry, as previously described [53,54]. Briefly, EVs isolated from 48h neutrophils (Ly6G+) cells culture were stained with antibodies in a 1:100 dilution in filtered PBS for 20 min on ice. To remove unbound antibodies, a second round of EVs isolation using ExoQick was performed. Isolated EVs were processed freshly for flow cytometry analysis.

2.15.3. Cancer stem cell, EMT, and neutrophil markers

Cells were stained with fluorochrome-conjugated antibodies for cell surface antigens (CD44, CD24, ITGA5, ITGA6, ITGB4, CD11b or Ly6G) in FACS buffer (DPBS supplemented with 2 % FBS and 1 % penicillin/streptomycin) at 1:100 for 30 min at 4 °C in the dark. Next, cells were fixed with 4 % Formalin and incubated at 4 °C in the dark until analysis. For the ALDH1A1 stain (stem cell marker), cells were stained with AIDeSense live-cell dye [70] for 30 min at 4 °C in the dark with 2uM (dissolved in DMSO) dye. Samples were washed serially with FACS buffer and resuspended in FACS buffer for analysis. Cytometry data were acquired, and cell status was determined.

2.16. Tumorsphere assay

Tumorsphere assay was performed according to a previously reported protocol [71]. Briefly, 1K of cells were seeded in ultra-low binding 24-well plates in 1 mL 0.5 % methylcellulose media supplemented with B27 (Gibco), epidermal growth factor (Corning), hydrocortisone (Sigma), insulin (Gibco), and B-ME (Sigma). On the seeding day, treatment with different doses of sEVs from DMSO or 27HC conditioned neutrophils were added. Sphere formation was evaluated under light microscope after 7 and 14 days and calculated using ImageJ software [72].

2.17. Migration assay

For migration assays, we used cancer cells after the sEVs treatment (see: *CANCER CELL TREATMENT WITH SMALL EXTRACELLULAR VESICLES*). Cells were seeded in EV depleted DMEM media on the top of 6.5 mm 8um PET membrane in 24well plates for 24h. In the bottom of the wells was complete DMEM with normal (non-EV depleted) FBS. Migrated cells on the membrane were fixed and stained with 0.2 % crystal violet according to the manufacturer's protocol. Images were acquired at 2× magnification using an EVOS XL Digital Inverted Brightfield and Phase Contrast Microscope (Invitrogen, USA) and analyzed using ImageJ software [72].

2.18. 3D tumorsphere proliferation assay

3D proliferation assay was performed as previously described [73] and schematically presented in Supplementary Fig. 7C&D. Briefly, 50 μL of Matrigel was used to coat the wells in 96-well plate and incubated for 30 min in 37 °C. 2000 cells were resuspended 100uL of complete DMEM with FBS EVs depleted media, supplemented with 2 % Matrigel. After 24h, cells were treated daily with DMSO-sEVs and 27HC-sEVs. After three days, Doxorubicin at 2 μM or Paclitaxel at 100 nM, or 1uM were added and proliferation was measured by bioluminescence readout (areascan 3x3, gain 200) using Synergy LX Plate Reader (Agilent, USA).

2.19. RNA-SEQ

Construction of the RNAseq libraries and sequencing on the Illumina NovaSeq 6000 were performed at the Roy J. Carver Biotechnology Center at the University of Illinois at Urbana-Champaign.

2.19.1. Construction of strand-specific RNAseq libraries

Total RNA was quantitated with Qubit high-sensitivity RNA reagent (Thermo Fisher) and the integrity and absence of genomic DNA was evaluated in a Fragment Analyzer (Agilent). The total RNAs were converted into individually barcoded polyadenylated mRNAseq libraries with the Kapa HyperPrep mRNA kit (Roche). Libraries were barcoded with Unique Dual Indexes (UDI's) which have been developed to prevent index switching. The adaptor-ligated double-stranded cDNAs were amplified by PCR for 10 cycles with the Kapa HiFi polymerase (Roche). The final libraries were quantitated with Qubit (Thermo Fisher) and the average cDNA fragment sizes were determined on a Fragment Analyzer. The libraries were diluted to 5 nM and further quantitated by qPCR on a CFX Connect Real-Time qPCR system (Bio-Rad) for accurate pooling of barcoded libraries and maximization of number of clusters in the flowcell.

2.19.2. Sequencing of libraries in the NovaSeq

The barcoded RNAseq libraries were loaded on one S1 lane on a NovaSeq 6000 for cluster formation and sequencing. The libraries were sequenced from both ends of the fragments for a total of 150bp from each end. The fastq read files were generated and demultiplexed with the bcl2fastq v2.20 Conversion Software (Illumina).

2.19.3. Quality check, alignment and counts of RNA-seq

All reference files were downloaded from NCBI's ftp site (https://ftp.ncbi.nlm.nih.gov/genomes/all/GCF/000/001/635/GCF_000001635.27_GRCm39/). The *Mus musculus* transcriptome file "GCF_000001635.27_GRCm39_rna.fna.gz" from Annotation 109 (https://www.ncbi.nlm.nih.gov/genome/annotation_euk/Mus_musculus/109/) from NCBI (https://www.ncbi.nlm.nih.gov/datasets/taxonomy/10090/) was used for quasi-mapping and count generation. This transcriptome is derived from genome GRCm39; Since the quasi-mapping step only uses transcript sequences, the gene model file "GGCF_000001635.27_GRCm39_genomic.gff.gz" was solely used to generate transcript-gene mapping table for obtaining gene-level counts.

The QC report was performed FASTQC (version 0.11.8, https://www.bioinformatics.babraham.ac.uk/projects/fastqc/) on individual samples then summarized into a single html report by using MultiQC [74] (https://multiqc.info) version 1.11. The average per-base read quality scores are over 30 in all samples and no adapter sequences were found indicating those reads are high in quality. Thus, the trimming step was skipped, and sequences were directly proceeded to transcripts mapping and quantification.

Salmon version 1.10.0 was used to quasi-map reads to the transcriptome and quantify the abundance of each transcript [75]. The transcriptome was first indexed using the decoy-aware method in Salmon with the entire genome file "GCF_000001635.27_GRCm39_genomic.fna.gz" as the decoy sequence. Then quasi-mapping was performed to map reads to the transcriptome with additional arguments –seqBias and –gcBias to correct sequence-specific and GC content biases, –numBootstraps = 30 to compute bootstrap transcript abundance estimates and –validateMappings and –recoverOrphans to help improve the accuracy of mappings. Gene-level counts were then estimated based on transcript-level counts using the "lengthScaledTPM" method from the tximport package. This method provides more accurate gene-level counts estimates and keeps multi-mapped reads in the analysis compared to traditional alignment-based method [76]. RNA-Seq data has been submitted to the NCBI Gene Expression Omnibus (accession number: GSE272476).

2.19.4. Statistical analysis of RNA-seq

When comparing expression levels, the numbers of reads per gene need to be normalized not only because of the differences in total number of reads, but because there could be differences in RNA composition such that the total number of reads would not be expected to be the same. The TMM (trimmed mean of M values) normalization [67] in the edgeR package [68] uses the assumption of *most genes do not change* to calculate a normalization factor for each sample to adjust for such biases in RNA composition.

Multidimensional scaling in the limma package [77] was used as a sample QC step to check for outliers or batch effects. Differential gene expression (DE) analysis was performed using the limma-trend method [78]. First, an F-test was performed to identify genes that changed anywhere across any of the 6 treatments by comparing each of the groups back to D_A.48 as the baseline.

2.19.5. Downstream analysis of RNA-seq

Weighted gene co-expression network analysis (WGCNA) is a data mining method developed to discover the co-expressed gene clusters (modules) and detect the core genes (hub genes) in each module [79]. Specifically designed R package was used for this analysis [80]. The soft thresholding power β was set to 5 to ensure a correlation coefficient close to 0.8. 16 modules were detected, and module heatmaps were plotted to visualize the expression pattern. Module eigengenes (ME) were calculated and visualized to represent the gene expression signatures of each module. Module membership (MM/kME) and gene significance (GS) were assessed for each module to understand the correlation of a gene to a module, and to assess the biological important of each gene accordingly. Upon identifying the module that shows significant different expression pattern between treatment groups, further analysis on gene enrichment, pathway, and clinical phenotype was performed using Shiny GO 0.80 version [81].

2.20. Clinical data analysis

Data used for analysis of breast cancer patient gene expression was downloaded from the cBioPortal (https://www.cbioportal.org/) (Breast Invasive Carcinoma, TCGA, Firehose Legacy), based on mRNA expression (RNA Seq V2 RSEM dataset). Spearman correlation was used for gene expression analysis using R ggpubr package (https://rpkgs.datanovia.com/ggpubr/) and/or Graphpad Prism. Signatures for EMT or stemness (CS) were generated, where the score was calculated based on median expression for each gene in the signature. EMT signature: VIM, SNAI1, SNAI2. CSC signature: SOX2, POU5F1 (OCT4), NANOG, CD44.

4. Results

From henceforth, sEVs obtained from neutrophils (Ly6G positive cells isolated from bone marrow) treated with vehicle (DMSO) will be referred to as DMSO-sEVs, and, sEVs obtained from neutrophils treated with 27HC will be referred to as 27HC-sEVs.

4.1. Chronic treatment of cancer cells with small extracellular vesicles from 27-hydroxycholesterol treated neutrophils (27HC-sEVs) leads to loss of adherence

We have previously shown that 27HC treatment of myeloid cells increased sEV biogenesis [53,54]. Another report found that the cholesterol-derived metabolite, dendrogenin A, increased sEV secretion from tumor cells by modulating the activity of the LXR [82]. While 27HC resulted in sEVs from neutrophils that increased tumor growth and metastasis [53], dendrogenin A treatment of cancer cells resulted in sEVs that were immunogenic and anti-cancer [82]. Neutrophil enrichment from bone marrow resulted in 93 % CD11B+; Ly6G + cells (flow cytometry gating strategy in Supplementary Fig. 1A). We confirmed that 27HC or dendrogenin A increased sEV secretion from neutrophils (sEV characterization in Supplementary Fig. 1B–C, sEV secretion in Supplementary Fig. 2A). Interestingly, other synthetic or endogenous LXR ligands had no effect on sEV secretion from these Ly6G + neutrophils (Supplementary Fig. 2A). Our previous work also found that cancer cells were able to take up 27HC-sEVs, suggesting that they may be a primary target [53].

To start elucidating the mechanisms by which 27HC-sEVs promote tumor progression, we performed an in vitro experiment, where we constantly exposed cancer cells to sEVs from neutrophils, mimicking the chronic exposure one would expect in the TME. We conducted this experiment in two independent TNBC murine cell lines: 4T1 and EMT6. The 4T1 cell line was derived from 410.4 tumor originating from the spontaneous mammary tumor of a BALB/c mouse, which closely resembles stage IV of human breast cancer [83]. The EMT6 cell line is a mammary murine carcinoma derived from BALB/c mouse [84]. Both lines are metastatic, with lesions found primarily in the lungs.

Cancer cells were treated with sEVs isolated from conditioned media of neutrophils treated with either vehicle (DMSO) or 27HC (experimental overview in Fig. 1A). To our surprise, the cancer cells exposed to 27HC-sEVs started to detach from the plates (Fig. 1B and C). The kinetics of detachment varied with 4T1 seeing peek detachment at 72h and EMT6 at 48h. To quantify this phenomenon, we determined the fraction of detached and attached cells using trypan blue exclusion to assess only live cells. There was a statistically significant difference between detached and attached 4T1 cells treated with 27HC-sEVs compared to DMSO-sEVs (Fig. 1D). Both live and dead cells were found attached and de-attached, for both treatment groups (Fig. 1E). When comparing adherent to non-adherent cells from 27HC-sEVs treatment, there was a slight increase in the proportion of dead cells in the non-adherent fraction, but this did not account for a large increase in non-adherent cells after this treatment (Fig. 1E and F). Moreover, when comparing live-adherent to live-non-adherent cells in our treatment groups, we found that treatment with 27HC-sEVs increased the live-non-adherent subpopulation (Fig. 1E and F). Importantly, the loss of adherence was conserved in a second cell line examined (EMT6, Fig. 1C–G-I). For EMT6 cells, the non-adherent fractions for both treatments had increased dead cells compared to the adherent, providing further evidence that the detachment effect of 27HC-sEVs was not due to an overall increase in cellular death (Fig. 1I). The fraction of live-non-adherent cells was significantly larger in EMT6 cells treated with 27HC-sEVs (Fig. 1H and I). Interestingly, when surveying other synthetic and endogenous LXR ligands, only 27HC-sEVs resulted in a significant loss of adherence (Supplementary Fig. 2B). In order to assess whether our observed loss of adherence was also apparent in luminal A, estrogen receptor alpha positive cells, we tested the effects of 27HC-sEVs on human MCF7 cells. 27HC-sEVs also resulted in loss of adherence of MCF7 cells (Supplementary Fig. 3).

To further rule-out whether 27HC-sEVs were inducing cellular death resulting in detachment, we evaluated apoptosis by staining with Annexin V-FITC and propidium iodide (PI) (gating strategy is presented in Supplementary Fig. 4A–B). Annexin V binds to phosphatidylserine, a membrane lipid that becomes accessible on the outer layer during cell membrane disruption. PI binds to DNA after entering the cell through an already disrupted membrane. It is important to note that although there were some non-adherent cells found in the media after treatment with DMSO-sEVs, the total number was too low to process with Annexin V/PI staining. Treatment with 27HC-sEVs did increase cells in the early and late apoptosis, in both remaining adherent and non-adherent 4T1 cells (Fig. 1J). This mirrors an accepted paradigm in vivo where the majority of cells intravasating do not survive, but a small population does which goes on to form metastatic lesions [85]. A similar, however distinct effect was observed in the EMT6 cell line after 48h of the treatments, with a significant subpopulation of live cells (Annexin V-/PI-) after treatment with 27HC-sEVs in comparison to DMSO-sEVs (Fig. 1K). For both cell types, there was also a significant fraction of live, non-adherent cells (Fig. 1J and K). 27HC treatment of neutrophils increases EV secretion by approximately 2-fold (Supplementary Fig. 1B and Supplementary Fig. 2A). However, treatment of 4T1 cells with two times the number of DMSO-sEVs did not increase loss of adherence to the extent of 27HC-sEVs (Supplementary Fig. 5A). Likewise, treating 4T1 cells with only 30 % of the sEV dose still resulted in an increase of non-adherent cells although at lower levels (Supplementary Fig. 5B). Furthermore, a single dose of 27HC-sEVs was sufficient to stimulate a loss of adherence (Supplementary Fig. 5C). Collectively, these data indicate that 27HC-sEVs uniquely promote cancer cell loss of adherence compared to DMSO-sEVs.

4.2. sEVs from 27HC-treated neutrophils promote pluripotency and stemness in cancer cells

Loss of adherence is a feature of stemness and/or epithelial to mesenchymal transition (EMT). Therefore, we assessed whether 27HC-

sEVs were influencing either stemness or EMT. We started by evaluating the expression of transcription factors known to play central roles in driving key transcriptional programs related to pluripotency and stemness: SOX2, OCT4, and NANOG [86]. As anticipated, the expression of SOX2, OCT4, and NANOG were upregulated in the resulting non-adherent 4T1 cells 72h after exposure to 27HC-sEVs (Supplementary Fig. 6A). Since we observed loss of adherence in EMT6 cells sooner (48h timepoint; Fig. 1), we examined this timepoint for changes in these transcription factors for EMT6. Similar to our findings in 4T1 cells, 27HC-sEVs increased the expression of SOX2, NANOG, and OCT4 (Supplementary Fig. 6B). For both cell types, the remaining adherent cells post 27HC-sEVs treatment also had higher expression of these transcription factors compared to DMSO-sEVs, resembling an intermediate state (Supplementary Fig. 6A–B). Gaining pluripotent ability (by overexpression SOX2, OCT4, and NANOG) by cancer cells can give rise to multiple types of cells within the tumor, contributing to tumor heterogeneity and chemoresistance [86–88].

Proliferative capacity is often low or reduced in stem-like cells [89]. As expected, we observed significantly reduced expression of the proliferation marker, ki67, through time in 27HC-sEVs treated 4T1 and EMT6 cells (Supplementary Fig. 6C–D). The reduction in ki67 was most pronounced in non-adherent populations, which emerged at 72h or 48h post-treatment for 4T1 and EMT6 cells, respectively. This suggests that 27HC-sEVs from neutrophils were indeed promoting stemness.

Cancer stem cells in human breast tumors have been characterized as $Lin^{neg}/CD24^{neg\ to\ lo}/CD44^{+}$ phenotype [90]. Murine mammary cancer stem cells have also been described to highly express CD44 and lose expression of CD24 [91]. CD44 is one of the regulators of self-renewal, tumor initiation and metastatic progression, and chemoresistance properties of cancer stem cells [92]. On the other hand, CD24 is a negative regulator of CXCR4; $CD24^{neg\ to\ low}$ phenotype upregulates CXCR4 and may give rise to increased migration activity, required for tumor initiation and metastatic progression [93]. A distinct breast cancer stem cell population was also identified and characterized by high activity of aldehyde dehydrogenase (ALDH), characterized by self-renewal capacity and multidrug resistance [94]. Moreover, the ALDH1A1 isoform is considered the main cancer stem cell-related isoform [95]. Based on the markers (ALDH, CD44, and CD24), breast cancer stem cells have been divided into subpopulations: epithelial-like, with $ALDH1A1^{+}$ $CD24^{neg\ to\ low}/CD44^{+}$, and mesenchymal-like, $ALDH1A1^{negative}$ $CD24^{neg\ to\ low}/CD44^{+}$ [91,96]. Our flow cytometric analysis of 4T1 or EMT6 cells after exposure to 27HC-sEVs revealed a robust enrichment of the $CD24^{neg}/CD44^{+}$ population (Fig. 2A and B). In addition, the expression of the ALDH1A1 marker decreased after 27HC-sEVs treatment in adherent and non-adherent 4T1 or EMT6 cells (Fig. 2C and D). The decrease in ALDH1A1 was most apparent in non-adherent cells at later timepoints (times after detachment was observed; Supplementary Fig. 6E–F). This indicates that after exposure to 27HC-sEVs, cancer cells are enriched in mesenchymal-like stem-like cancer cell subpopulations characterized by $ALDH1A1^{negative}$ $CD24^{neg}/CD44^{+}$.

A hallmark of stem-like cells is their ability to grow in an anchorage-independent fashion [97]. Therefore, we tested the ability of cancer cells to form tumorspheres in the presence of DMSO-sEVs or 27HC-sEVs. The assay was conducted for a total of 14 days with two assessment points – 7 and 14 days (Fig. 2E–J, Supplementary Fig. 6G). There was no statistical difference in the total number of tumorspheres between treatment groups (Fig. 2E and F) for both tested time points; with the exception of the no-treated group which was lower than the smallest dose of DMSO-sEVs neutrophils (7 days, Fig. 2E). However, there was a decrease in surviving tumorspheres between 7 days and 14 days of culture (Fig. 2E–G). The rate of this decrease was not as pronounced in tumorspheres treated with 27HC-sEVs (Fig. 2G). In contrast, the rate of tumorsphere loss was apparent in all doses of DMSO-sEVs examined (Fig. 2G).

Interestingly, we also observed larger diameters in 4T1 tumorspheres formed in the presence of 27HC-sEVs compared to DMSO-sEVs for both tested time points (Fig. 2H and I). Linear regression (Fig. 2J) revealed a dose-dependent growth of tumorspheres after 27HC-sEVs and DMSO-sEVs treatments.

Overall, sEVs from 27HC-treated neutrophils upregulate the main transcription factors associated with pluripotency in mammary cancer cells. At the cellular level, mammary cancer cells treated with 27HC-sEVs gain a mesenchymal stem-like phenotype ($ALDH1A1^{negative}$ $CD24^{neg}/CD44^{+}$) suggestive of epithelial-mesenchymal transition and, in consequence, lose their adherence.

4.3. sEVs from 27HC treated neutrophils alter epithelial-mesenchymal transition in recipient cancer cells

Loss of adhesion is one of the hallmarks of metastasis [98]. In general, epithelial cancer cells lose dependence on integrin-mediated and cadherin-dependent interactions with extracellular matrix and cell-to-cell adhesion. For that reason, we evaluated this phenomenon after sEVs treatments.

EMT is a reversible process that allows epithelial cells to adopt a mesenchymal state [96]. The “cadherin switch” is a characteristic movement assigned to the EMT. It is manifested by loss of E-cadherin (CDH1) expression and increased N-cadherin (CDH2) expression accompanied by different integrin changes. The downregulation of *Cdh1* and upregulation of *Cdh2* was observed in 4T1 cells after 72h and 96h treatment with 27HC-sEVs for both subpopulations: attached and non-adherent cells (Fig. 3A and B). *CDH1* protein was also decreased (Fig. 3E). EMT6 cells showed an increase in CDH1 mRNA and protein (Fig. 3C,D&F). Gain of CDH2 is a hallmark of EMT. Both 4T1 and EMT6 cells had increased *Cdh2* expression after treatment with 27HC-sEVs (Fig. 3A–D). The expression of other genes associated with EMT were also altered in in both cell lines (Fig. 3A–D). Collectively, these data suggest that 27HC-sEVs push breast cancer cells into a state closer to mesenchymal cells on the spectrum between epithelial and mesenchymal states, which is a common phenomenon for cancer cells [96].

Integrins are transmembrane adhesion molecules that mediate signals between extracellular matrix and the cytoskeleton. Upon activation, they are able to change cell gene expression, polarity, proliferation, migration, and phenotype. The integrin superfamily consists of 18 α and 8 β units, which can combine to form 24 functional heterodimers. Notably, α5 subunit is recognized as a mediator of metastatic progression in solid tumors, including breast cancer [99]. Subunit α6 often parried with β4, is recognized as a stemness marker [100]. ITGα5 levels were increased in both 4T1 and EMT6 cells after detachment due to 27HC-sEV treatment (Fig. 3E and F). ITGβ4 and ITGα6 were both decreased in 4T1 cells but increased in EMT6 cells (Fig. 3E and F). This pattern aligns with the known role of α6 and β4 in maintaining epithelial-like phenotype, facilitating epithelial adhesion and epithelial stability [101]. mRNA levels for these integrins did not always reflect protein levels (Supplementary Fig. 7A–B). Collectively, our data suggest that 27HC-sEVs push cancer cells into EMT, with resulting gene and protein expression of cadherins and integrins indicating cells in between complete transition.

Stem and mesenchymal-like populations of cancer cells tend to be migratory [102,103]. To investigate the migratory ability of cancer cells after the sEVs treatments, we took detached subpopulations of cells after treatment with DMSO-sEVs or 27HC-sEVs and assessed their ability to migrate through a Boyden chamber. For both 4T1 and EMT6 cancer cells, we observed increased migration in cells treated with 27HC-sEVs, with the highest migration in loose-adherent (transitioning) 27HC-sEVs treated cells (Fig. 4A and B). This increased migration may explain the previously observed increased metastatic colonization/outgrowth observed when 27HC-sEVs were administered to mice [53].

Another feature of stem cancer cells and EMT is resistance to cytotoxic chemotherapy. Drug resistance was assessed by 3D proliferation of 4T1 tumor spheroids co-treated with DMSO-sEVs or 27HC-sEVs and

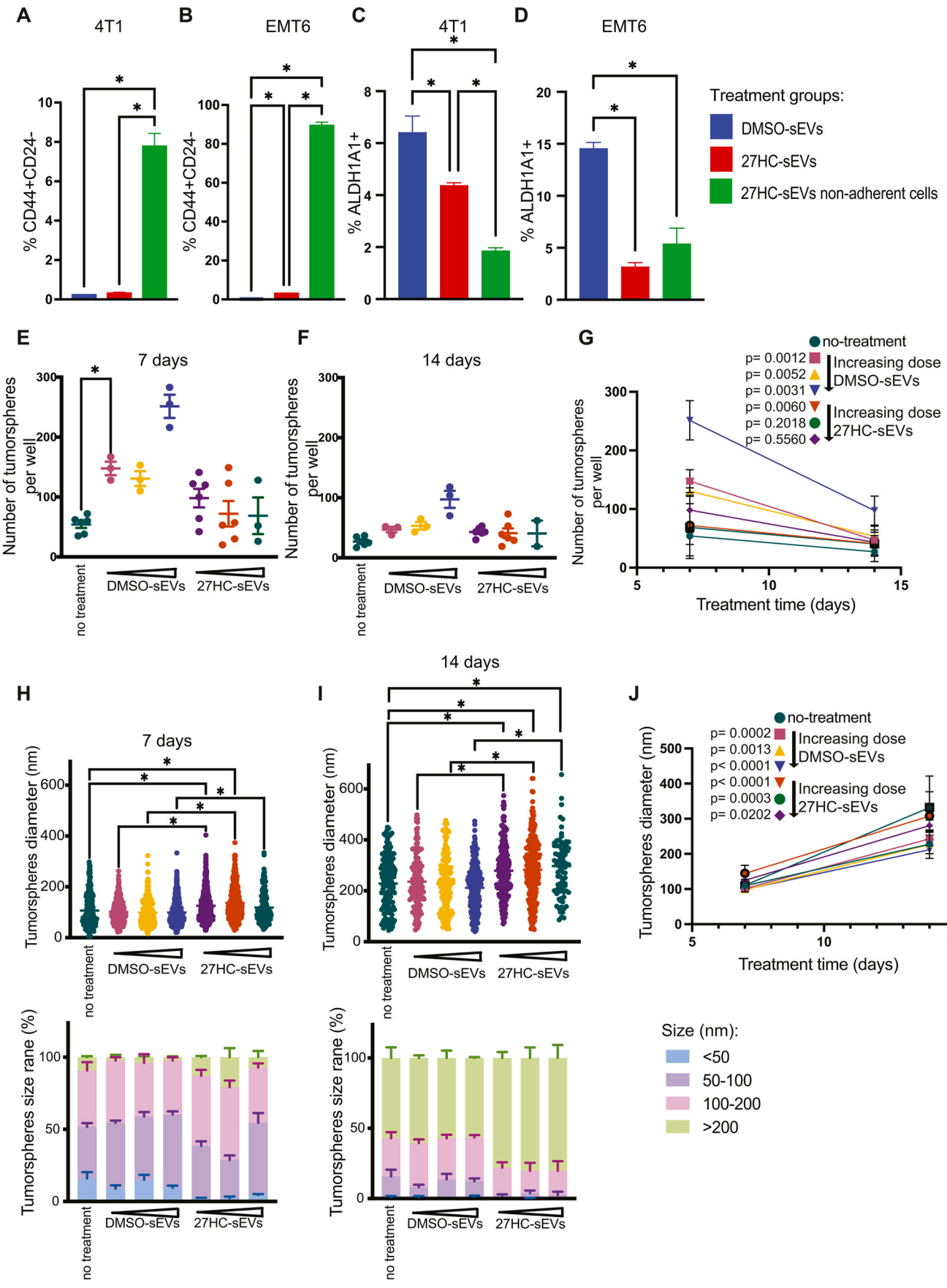

(caption on next page)

Fig. 2. ***Treatment of mammary cancer cells with 27HC-sEVs from neutrophils results in a stem-like phenotype.*** **(A–B)** Flow cytometry quantification of $CD44^+/CD24^-$ cells of **(A)** 4T1 after 72h and **(B)** EMT6 after 48h exposure to DMSO-sEVs or 27HC-sEVs. **(C–D)** Flow cytometry quantification of $ALDH1A1^+$ cells of **(C)** 4T1 after 72h and **(D)** EMT6 after 48h of exposure to DMSO-sEVs or 27HC-sEVs. **(E–G)** Quantification of 4T1 tumorspheres after 7 days **(E)** and 14 days **(F)** of culture with different doses of DMSO-sEVs and 27HC-sEVs. **(G)** Linear regression of 4T1 tumorsphere number after 7 days and 14 days of culture with different doses of DMSO-sEVs and 27HC-sEVs. **(H–J)** Quantification of 4T1 tumorsphere diameters after 7 days **(H)** and 14 days **(I)** of culture with different doses of DMSO-sEVs and 27HC-sEVs. **(J)** Linear regression of 4T1 tumorsphere diameters from 7 days to 14 days of culture with different doses of DMSO-sEVs and 27HC-sEVs. All data are presented as mean ± SEM. Statistical analyses (**A-D**, N = 3; **E-F, H-I**, N = 3–6/treatment group) were performed using one-way ANOVA followed by Tukey's multiple comparison test, with an asterisk (*) indicating $P < 0.05$.

doxorubicin (DOX), paclitaxel (PAC) or vehicle (DMSO) through time. As expected, growth of 4T1 spheroids treated with DMSO-sEVs were inhibited by DOX or paclitaxel treatment (Fig. 4C and D, experimental setup in Supplementary Fig. 7C–D). In contrast, 4T1 spheroids treated with 27HC-sEVs were not sensitive to DOX or paclitaxel treatment (Fig. 4C and D). Similar chemoresistance was observed in EMT6 spheroids treated with 27HC-sEVs (Fig. 4E and F).

In order to highlight the relevance of our findings to human tumors we have performed correlational analyses to CYP27A1, the enzyme responsible for converting cholesterol to 27HC. Thus, one would expect higher local 27HC concentrations in tissue with elevated CYP27A1 expression [104]. We observed a negative correlation between *CYP27A1* and *GSK3*β; in the absence of WNT signaling, GSK3β results in the degradation of β-catenin (Fig. 4G, TCGA Breast Invasive Carcinoma, Firehose Legacy). We next generated EMT- and cancer stem cell (CSC)-gene signatures (EMT: *VIM, SNAI1* and *SNAI2*; CSC: *SOX2, POU5F1* (*OCT4*), *NANOG* and *CD44*). There was a positive correlation between *CYP27A1* and both the EMT and CSC gene signatures, and also an inverse correlation to *CDH1*; CDH1 loss being a characteristic of mesenchymal cells (Fig. 4H–J). Correlations between CYP27A1 and the individual genes of these signatures are shown in Supplementary Fig. 8. These correlations in human breast tumors support data obtained from murine models, and reinforce the clinical relevance of our findings.

Collectively, these data strongly suggest that exposure to 27HC-sEVs initiates EMT and increased stemness. This allows cancer cells to detach from the plates, form persistent and larger tumorspheres, gain migratory ability and resist cytotoxic chemotherapies, all important features in the metastatic progression cascade.

4.4. sEVs from 27HC-treated neutrophils disrupt the WNT/β-catenin pathway and impact stem-like properties in recipient cancer cells

To better understand the mechanisms of how 27HC-sEVs promoted loss of adherence, stemness and EMT, we performed a nonbiased, bulk RNA-Seq on 4T1 mammary cancer cell after exposure to DMSO-sEVs or 27HC-sEVs. To best capture dynamic regulation by sEVs cargo, we evaluated two-time points and powered these studies with five replicates per group. For cells exposed to 27HC-sEVs, we performed RNA-Seq on both cells that lost their adherence (non-adherent) and those that remained attached to the plate (adherent).

Using two-way ANOVA with an FDR cutoff of 0.05, 11,637 genes were found to be differentially expressed (DEGs) between the six groups (Fig. 5A). As illustrated by a Multidimensional Scaling Plot (MDS), exposure of 4T1 cells to 27HC-sEVs resulted in a unique transcriptional landscape compared to DMSO-sEVs; the most variance between groups being described by dimensions 1 and 2 (Fig. 5B). Within each treatment type, a shift in dimension 1 and 2 were observed through time (Fig. 5B). For those cells treated with 27HC-sEVs, both adherent and non-adherent cells clustered separately from those treated with DMSO-sEVs, particularly along dimension 1 (Fig. 5B). At the second timepoint (72h), the adherent cells treated with 27HC-sEVs started to more closely resemble nonadherent ones at the first timepoint (48h). Raw gene counts (Gene-Level_counts), and logarithmic counts per million reads of the trimmed mean of M-values (TMMnormalized_logCPM) are listed in **Supplementary Datasheet 1.**

The time, treatment, and adherence variables in our experimental setup made it challenging to perform broad pathway analyses on the DEGs. Therefore, to focus our evaluation of 4T1 expression patterns following treatment with neutrophil-derived sEVs, we utilized weighted gene co-expression network analysis (WGCNA). The soft thresholding power β was set to five to ensure a correlation coefficient close to 0.8. Therefore, $\beta = 5$ (Fig. 5C) was used to generate a hierarchical clustering tree (Fig. 5D). A total of 16 different color-coded co-expression modules were identified. Each module is depicted in Supplementary Fig. 9 and **Supplementary Datasheet 2**. Statistical analysis between treatment groups in specific modules (Supplementary Table 1) revealed the modules with the lowest P-value as Module 1 (co-downregulated genes, adj. P.Val = 6.80546234426343e-19) and Module 2 (co-upregulated genes, adj.P.Val = 1.55549927195221e-15) (Fig. 6A and B, Supplementary Datasheet 3). Corresponding heatmaps for each module are presented in Fig. 6C and D.

Gene-set enrichment analysis of Module 1 and Module 2 hub genes was performed using Shiny 0.8 [81]. Enrichment of genes associated with cell cycle was found in Module 1, with 27HC-sEVs resulting in their down-regulation (Fig. 6E). Interestingly, in 4T1 cells treated 27HC-sEVs, there was significant enrichment in genes associated with the WNT signaling and the pluripotency (Module 2, upregulated by 27HC-sEVs, Fig. 6F). Collectively, these analyses suggest that 27HC-sEVs downregulate the cell cycle and division process while increasing WNT signaling and pluripotency. It is recognized that decreased cell-cycle is a characteristic feature of cancer stem cells [87] and that WNT/β-catenin signaling is an important driver of pluripotency [105]. These data provide a potential mechanism for our observations that exposure of cancer cells to 27HC-sEVs lose their adherent properties, another common feature of pluripotent or stem-like cells [98]. Therefore, we focused on this pathway for further analysis.

4.5. sEVs from 27HC-treated neutrophils alter the expression of several genes in the WNT/β-catenin pathway

We first focused on the WNT/β-catenin pathway, as it has been implicated in EMT, driving stem-like states and loss of adherence [98, 106,107]. Therefore, we performed independent experiments examining both 4T1 and EMT6 cells exposed to sEVs for two different timeframes. Gene expression analysis of several genes involved in the WNT/β-catenin pathway found that many were altered, with the largest differences observed 27HC-sEVs treated cells that had lost their adherence (Supplementary Fig. 10). The expression of: WNT5A, WNT9B, WNT2B, FRZ3, FRZ6, CTNNB1, APC, AXIN2, TCF7 was increased. At the same time, GSK3b was decreased in 4T1 cells after 72h and 96h (Supplementary Fig. 10A) compared to cells treated with DMSO-sEVs. A similar pattern was observed in the EMT6 cell line after 48h and 72h (Supplementary Fig. 10B).

Glycogen synthase kinase-3b (GSK3b) negatively regulates the WNT/β-catenin pathway by promoting the phosphorylation and subsequent proteasomal degradation of β-catenin [108]. When GSK3b is inhibited, β-catenin accumulates in the cytoplasm and is translocated to the nucleus, where it functions as a co-transcriptional activator for T-cell factor/lymphoid enhancer factor (TCF/LEF) transcription factors, upregulating transcription of c-myc, WNT genes, and SOX2 [108,109]. In our case, GSK3b was downregulated by 27HC-sEVs, while β-catenin (CTNNβ1) was upregulated, reinforcing this signaling loop (Supplementary Fig. 10). In addition, other genes activating the pathway were upregulated by 27HC-sEVs. Collectively, these data

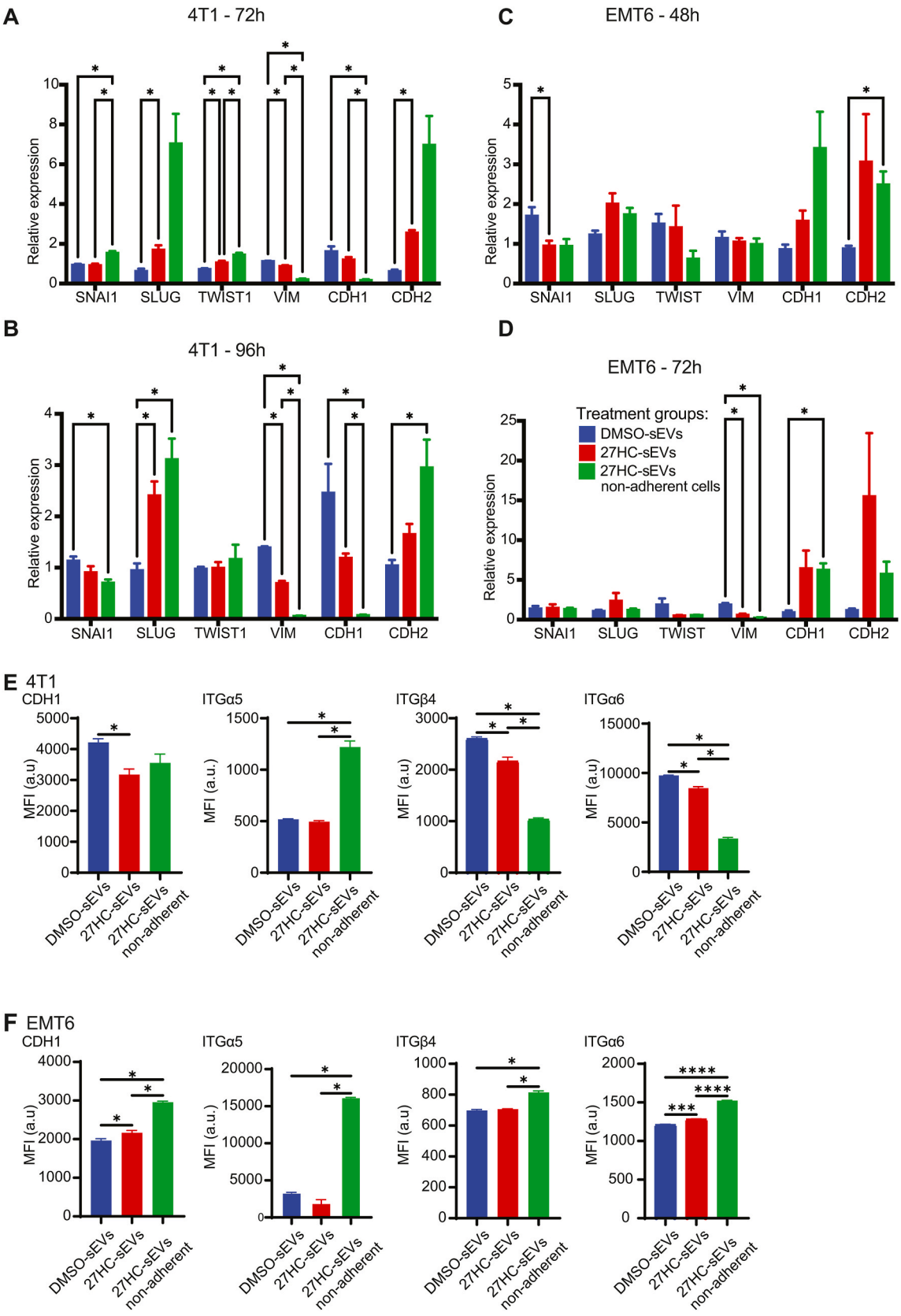

Fig. 3. *Treatment of mammary cancer cells with 27HC-sEVs from neutrophils results in an epithelial to mesenchymal transition (EMT) phenotype.*
(A–B) EMT gene expression patterns in 4T1 cells after exposure to DMSO-sEVs or 27HC-sEVs for 72h or 96h respectively. **(C–D)** EMT gene expression patterns in EMT6 cells after exposure to DMSO-sEVs or 27HC-sEVs for 48h and 72h respectively. **(E–F)** Flow cytometric quantification of CDH1, ITGα5, ITGβ4, and ITGα6 surface expression in 4T1 and EMT6 cells treated with DMSO-sEVs or 27HC-sEVs. Statistical analyses were performed using one-way ANOVA followed by Tukey's multiple comparison test, with an asterisk (*) indicating $P < 0.05$ (**A-D**, N= 5–6; **E-F**, N = 3/treatment group).

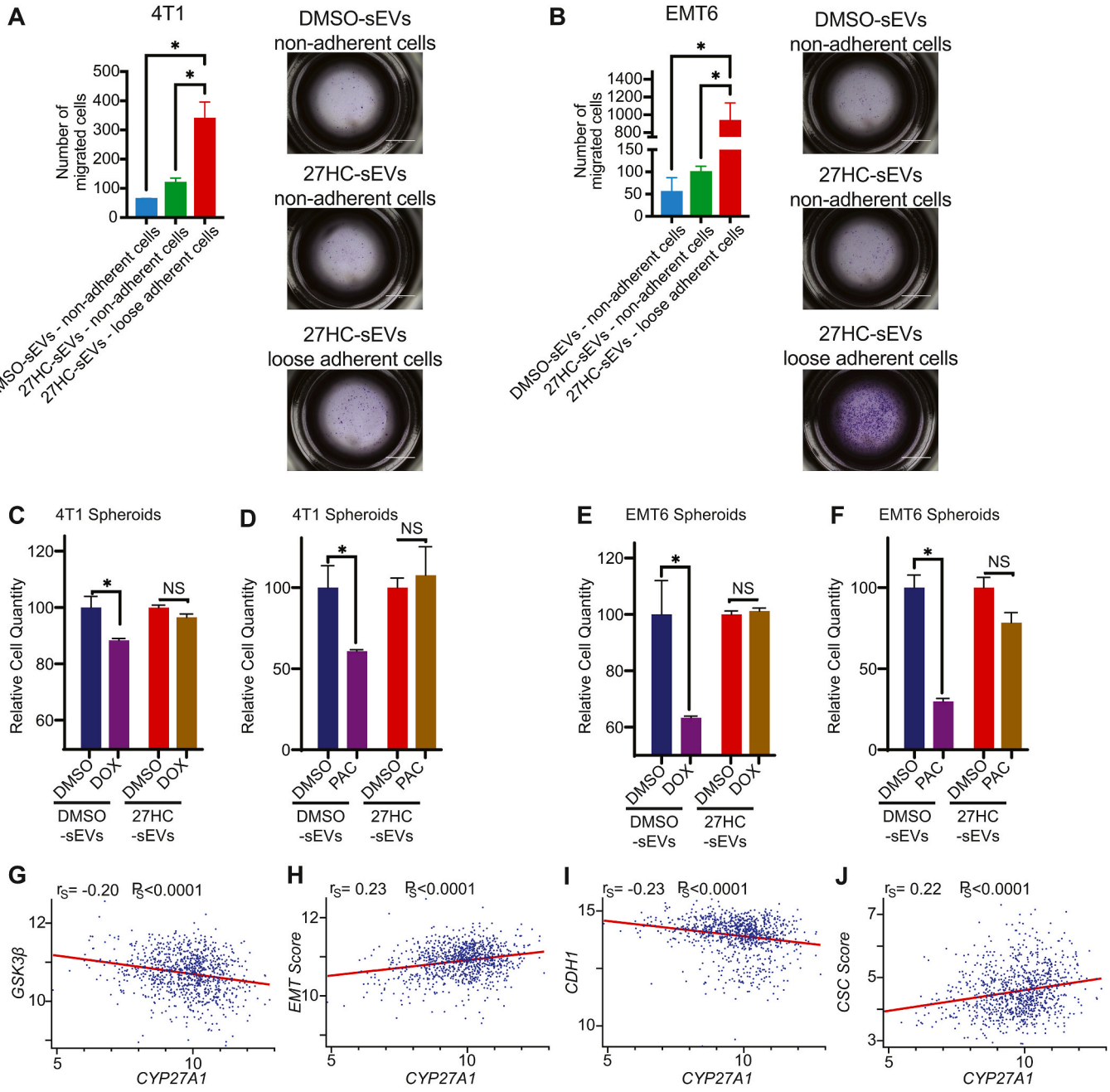

Fig. 4. *Treatment of mammary cancer cells with 27HC-sEVs from neutrophils results in increased migration and chemoresistance.*
(**A**) Quantification of migrated 4T1 cells. 4T1 cells were cultured in the presence of either DMSO-sEVs or 27HC-sEVs for 72h prior to seeding onto a Boydon Chamber and allowing to migrate for 24h. Representative pictures for each treatment are presented to the right of the quantified data. (**B**) Quantification of migrated EMT6 cells. EMT6 cells were cultured in the presence of either DMSO-sEVs or 27HC-sEVs for 48h prior to seeding onto a Boydon Chamber and allowing to migrate for 24h. Representative pictures for each treatment are presented to the right of the quantified data. Statistical analyses for A-B were performed using one-way ANOVA followed by Tukey's multiple comparison test, N = 3/treatment group, an asterisk (*) denoting $P < 0.05$ **(C–D)** Quantification of 4T1 and EMT6 spheroid cell quantity after 12 days (4T1 spheroids) or 20 days (EMT6 spheroids) of treatment with DMSO-sEVs or 27HC-sEVs in combination with either vehicle (DMSO) or 2uM doxorubicin. (A–F) All data are presented as mean ± SEM. **(E–F)** Quantification of 4T1 and EMT6 spheroid cell quantity after 12 days of treatment with DMSO-sEVs or 27HC-sEVs in combination with either vehicle (DMSO) or paclitaxel (4T1 spheroids - 100 nM; EMT6 spheroids - 1uM). Statistical analyses of C-F were performed using a students T test where each subgroup were compared to DMSO control, N = 3/treatment group, with an asterisk denoting $P < 0.05$. **(G)** Breast tumoral mRNA expression of *GSK3β* is negatively correlated with *CYP27A1* (RNA Seq v2 RSEM, from the Breast Invasive Carcinoma, TCGA, Firehose Legacy dataset). Linear regression was performed to generate the red line. Spearman's correlation indicated (r_s) along with the Spearman correlation P value (P_s). **(H–I)** An EMT gene signature was positively correlated while CDH1 expression was negatively correlated with *CYP27A1*. Details as for (G). **(J)** A cancer stem cell gene signature was positively correlated with *CYP27A1*. Details as for (G).

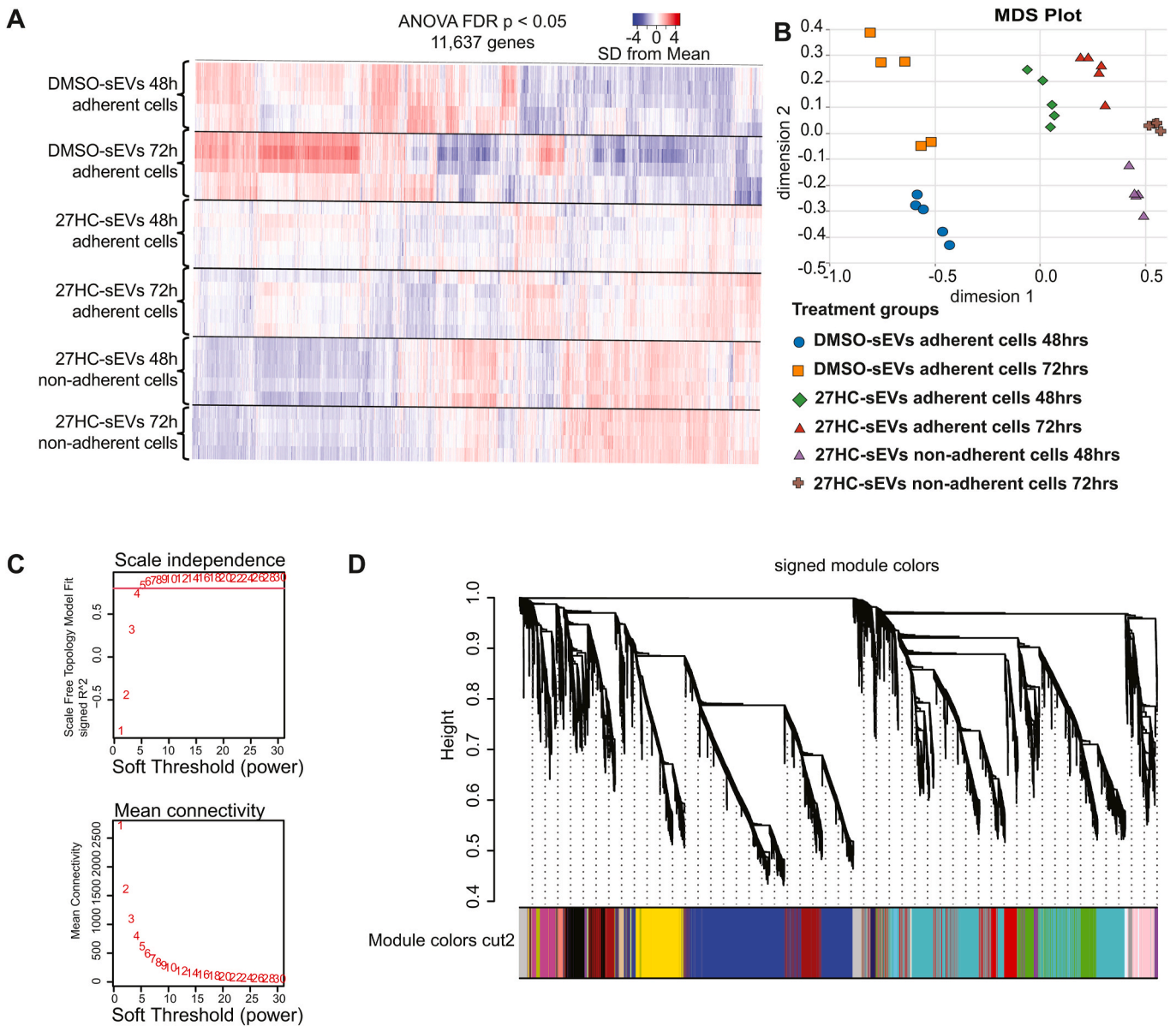

Fig. 5. ***Transcriptome of cancer cells significantly changes upon treatment with 27HC-sEVs.*** Murine neutrophils were treated with DMSO or 27HC followed by sEV isolation from the conditioned media. 4T1 cancer cells were exposed to the sEVs for 48h or 72h. Both adherent and non-adherent cells were harvested and sent for bulk RNA-Seq. **(A)** Heatmap of DEGs between all tested groups. Statistical analyses were performed using two-way ANOVA, FDR <0.05. N = 5 **(B)** MDS plot segregating and grouping samples based on dimensions 1 and 2. **(C)** WGCNA settings: The soft threshold power β settings are based on scale independence and mean connectivity. **(D)** WGCNA settings: a clustering diagram of the gene modules dendrogram by distinct colors. Each colored line represents a color-coded module containing highly connected genes. (For interpretation of the references to color in this figure legend, the reader is referred to the Web version of this article.)

indicate that 27HC-sEVs robustly increase WNT signaling in mammary cancer cells, suggesting that this may be a predominant pathway in the stemness and EMT phenotypes observed.

4.6. 27HC-sEVs carry small amounts of 27HC; concentrations that do not promote loss of adherence

Using simultaneous label-free autofluorescence multiharmonic (SLAM) microscopy, we previously found that sEVs from 27HC-treated neutrophils have a decreased FAD:(FAD + NAD(P)H) ratio compared with sEVs from DMSO-treated neutrophils [53,54]. This strongly suggested that there is a difference in the cargo of 27HC-sEVs compared to DMSO-sEVs. Therefore, in order to investigate the potential mechanisms behind loss of adherence after exposure to 27HC-sEVs (Fig. 1) and ultimately metastatic progression [53,54], we probed differences in the sEV molecular cargo, focusing on 27HC and RNA content.

Macrophages have been previously demonstrated to have high expression of CYP27A1, the enzyme responsible for the synthesis of 27HC from cholesterol [110,111]. Previous work using single cell RNA-seq revealed that neutrophils had significantly decreased CYP27A1 expression compared to macrophages or monocytes isolated from metastatic lungs or atherosclerotic plaques [39,111]. We confirmed these findings by assessing expression in bone marrow derived myeloid cells using RT-qPCR. Although neutrophils do express *Cyp27Aa1* mRNA, it is at much lower levels compared to bone marrow derived macrophages, peritoneal mast cells, or bone marrow derived dendritic cells; neutrophils expressing *Cyp27a1* to around the same degree as mast cells (Supplementary Fig. 11A). The enzyme that catabolizes 27HC, CYP7B1, was also explored. *Cyp7b1* was higher in granulocytes compared to macrophages or dendritic cells (Supplementary Fig. 11B). The fetal

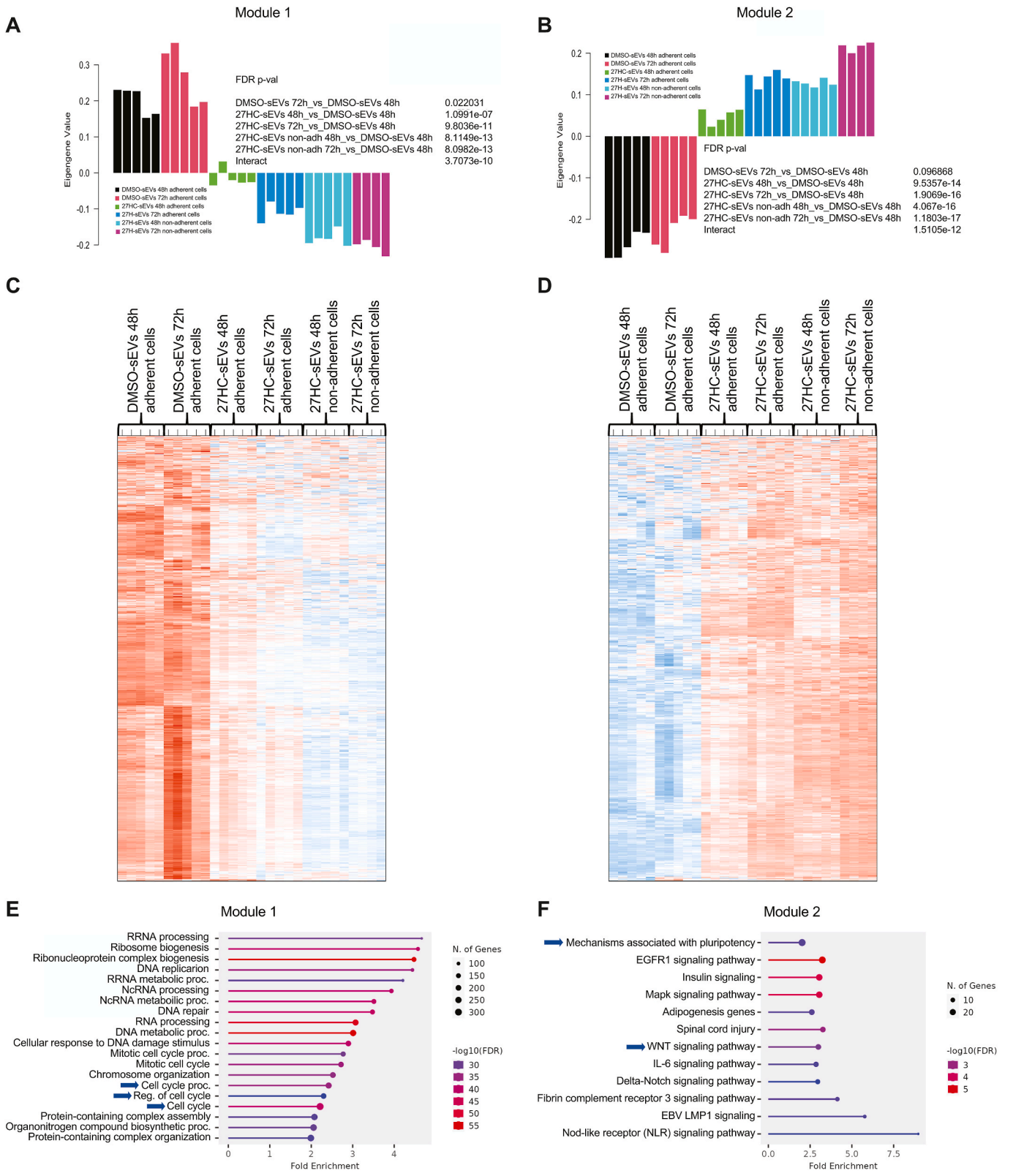

Fig. 6. ***WGCNA analysis reveals several distinct modules of DEGs, the two most robust being comprised of genes associated with cell cycle, pluripotency and WNT signaling.*** RNA-Seq data from Fig. 5 were analyzed by weighted gene co-expression network analysis. The two most prominent modules depicted here, the remaining in Supplementary Fig. 9. **(A)** Module 1 co-downregulated genes – samples segregation. **(B)** Module 2 co-upregulated genes – samples segregation. **(C)** Module 1 – heatmap of co-downregulated genes between the treatment groups. **(D)** Module 2 – heatmap of co-upregulated genes between the treatment groups. **(E–F)** Module 1 and Module 2 gene set enrichment analysis respectively, based on Shiny 0.8 software.

bovine serum (FBS) used to culture neutrophils (sEV-free) and cancer cells was assessed for oxysterol content, but all those tested were below detection limits (Supplementary Fig. 11C details our positive controls; assessments were made in two independent facilities). To determine the capacity of neutrophils to synthesize 27HC, we cultured them with or without cholesterol and then quantified resulting 27HC in the conditioned media by LC-MS/MS. Resulting concentrations of 27HC were below detection limits (not shown). Thus, given the low *Cyp27a1* expression and undetectable 27HC after culture in the presence of cholesterol, we conclude that neutrophil capacity to generate 27HC is low.

Regardless of the capacity for neutrophils to synthesize their own 27HC, it was possible that 27HC was either being co-selected for with the sEVs isolation, or that 27HC was being enriched within the sEVs themselves and transferring that to cancer cells; both scenarios ultimately resulting in loss of adherence. To explore this further, we assessed the 27HC concentration of sEVs from DMSO or 27HC treated neutrophils. 27HC was detected in sEVs from 27HC-treated neutrophils

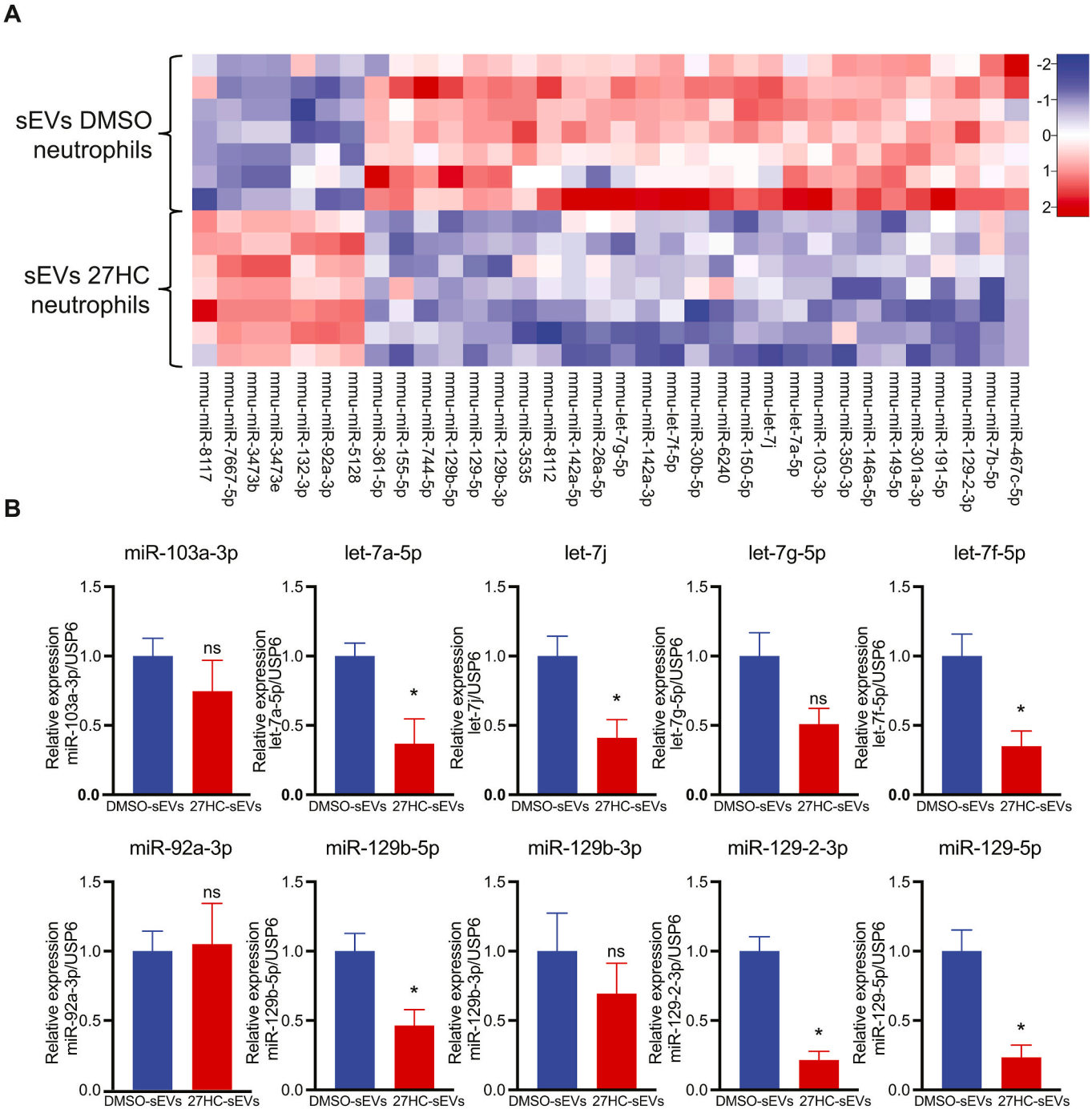

Fig. 7. ***miR cargo of sEVs is altered after 27-hydroxycholesterol treatment of parental neutrophils.*** Murine neutrophils were treated with 27HC. Secreted sEVs were isolated from the media and processed for small RNA-Seq. **(A)** Heatmap of statistically significant, differently expressed microRNAs between sEVs isolated after treatment with either DMSO or 27HC. The False Discovery Method was used for statistical analysis. N = 7/group **(B)** microRNA transcripts quantified by RT-qPCR from DMSO-sEVs and 27HC-sEVs. Statistical analyses were performed using Student's T-test. N = 3/treatment group, with an asterisk (*) denoting $P < 0.05$. Data are presented as mean ± SEM.

(Supplementary Fig. 11D).

We next performed an experiment where DMSO or 27HC were spiked in with neutrophils right before isolation of sEVs. These sEVs were then administered to 4T1 cells (Supplementary Fig. 11E). Adding 27HC at this time did not influence adherence, (Supplementary Fig. 11F). Furthermore, chronic exposure of cancer cells to 27HC alone at the same concentrations as those measured in 27HC-sEVs, did not result in loss of adherence (either 4T1 or EMT6 cells; Supplementary Fig. 11G–H). Collectively, these findings suggest that although 27HC-sEVs do carry 27HC, 27HC itself is not sufficient to drive a biological response, but rather that other sEV cargo was mediating responses in cancer cells.

4.7. Elevated 27HC modulates the miR content of small extracellular vesicles isolated from neutrophils

Our finding that 27HC transfer did not alter adherence led us to believe that other cargo were involved in mediating these effects. RNA is one of the major constituents of sEV cargo, and has significant regulatory capacity [112]. Therefore, we focused our efforts on RNA content.

Total RNA was isolated from DMSO-sEVs and 27HC-sEVs, using methods to also capture small amounts of RNA. First, we used Bioanalyzer 2100 (Agilent) and the Total RNA Pico kit detection method for fragment size, concentration, and quality verification. The RNA fragments were in the size range below 200 nucleotides (nt) (Supplementary Fig. 12A–B). The RNA integrity number (RIN) is based on the 28S:18S ratio, where a 2:1 ratio is considered the best RNA quality [113]. The observed relatively small or absent fragments of 18S and 28S in our tested samples highly suggest that the isolated RNA does not reflect the size distribution expected in a cell (as in, sEV RNA did not contain large RNA molecules, e.g. 18S and 28S). Thus, to evaluate the RNA species smaller than 200 nt, we performed a secondary analysis using the DNF-470-22 - Small RNA kit on an AATI Fragment Analyzer (Agilent). For all tested samples of total RNA isolated from sEVs, the detected fragments were in the range of 10-60 nt, with the average peak at 18 nt (Supplementary Fig. 12C–D). The calculated data revealed that, on average, 91.7 % of isolated RNA qualified as microRNA (miR).

Therefore, we next focused on characterizing the miR cargo by performing small RNA-Seq on isolated sEVs from treated neutrophils, we powered our study with N = 7 per group. In total, 1031 different miRs were detected in both treatment groups (Supplementary Fig. 12E). However, only 34 miRs were statistically differently expressed between the groups (Fig. 7A). Seven miRs were upregulated while 27 miRs were downregulated in 27HC-sEVs compared to DMSO-sEVs. We next validated our results in an independent experiment, employing the gold standard RT-qPCR method [114]. Since we could not assume that 27HC did not alter small RNAs typically used as internal controls, we decided to use an exogenous reference control by spiking – miR USP6 (Qiagen). As a further control, we assessed miR-103a-33p which was not found to be significantly regulated in the RNA-Seq, which was confirmed by qPCR (Fig. 7B). Our results confirmed the changes in several of the differentially expressed miRs identified by small RNA-Seq of sEVs (Fig. 7B). To better understand the potential impact of the identified differentially expressed miRs in recipient cancer cells, we used three different bioinformatics pipelines (described in the Methods section with an overview summary in Supplementary Fig. 13) to predict targeted pathways. Even though we were able to detect statistical differences in miR expression between our treatment groups (Fig. 7A), when considered individually the prediction of potential downstream pathways for each miR was not informative. Therefore, future analysis was conducted using clusters of miRs.

Based on this analysis, the downregulated miRs in 27HC-sEVs were predicted to have an impact on insulin signaling, response to hypoxia, GnRH signaling, PI3K-Akt-mTOR signaling, signaling pathways regulating pluripotency of stem cells, TGF-beta signaling, angiogenesis, EGF receptor signaling, WNT signaling, MAPK signaling pathways, response to amyloid-beta, oxidative stress response, and synaptic vesicle. Overall, 13 potential pathways that might be targeted by differentially expressed miRs were consistently implicated across the different bioinformatic approaches used (Supplementary Table 2). Gaining stem-like properties (e.g. pluripotency) by cancer cells was detected in two bioinformatic pipelines and caught our attention given our observations that 27HC-sEVs stimulated loss of adherence and our previous results described in this project. Gaining pluripotency or stem-like phenotypes may be driven by multiple pathways [105]. Our analysis of differential miRs predicted several downstream pathways that are implicated in driving pluripotency and 'stemness'. Specifically, the PI3K-Akt-mTOR, TGF-beta, WNT, MAPK, and hypoxia signaling pathways have all been previously implicated in breast cancer progression, metastasis, and drug resistance [105,115,116]. Given the fact, that bulk RNA-Seq on cancer recipient cells also implicate the WNT pathway; our bioinformatics analysis of potential targets of downregulated microRNAs strengthened our conclusions that this is the pathway leading to the gaining the stem-like phenotype by recipient cancer cells.

4.8. 27-Hydroxycholesterol also changes miR content of neutrophils, the cellular source of sEVs

It has been reported that the cargo of sEVs can be selectively loaded, as in their contents do not necessarily reflect those of their parental cells [117–119]. To better understand the origins of the differentially expressed miRs in sEVs, we simultaneously quantified select miRs in the parental neutrophils (Supplementary Fig. 14A) and resulting sEVs (Supplementary Fig. 14B). After 24h of treatment, miR expression levels in neutrophils had shifted but were not yet statistically significant (Supplementary Fig. 14A). At this timepoint, no changes were observed in sEVs apart from let-7j which was slightly upregulated (Supplementary Fig. 14B). Since many of the miRs of interest were downregulated by 27HC and miR turnover may take more than 24h, we next assessed a 48h timepoint. At this timepoint, the majority of miRs probed were significantly regulated by 27HC in neutrophils (Supplementary Fig. 14C). The differences observed in neutrophils 48h post-treatment were also reflected in the cargo of resulting sEVs (Supplementary Fig. 14D).

These results, comparing miR expression in neutrophils to sEVs, strongly suggest that 27HC modulates miR content within neutrophils themselves and that the miR cargo in sEVs is reflective of this change. However, the process may consist of multiple steps, and although our kinetic data would suggest the regulation of miRs primarily at the cellular level, we cannot rule out selective loading into sEVs. The mechanisms by which 27HC modulates miRs in the neutrophil or how they are loaded into sEVs require further investigation.

4.9. Let-7 miRs are a main regulatory component resulting in observed changes in recipient cancer cells

Even though we were able to detect statistical differences in the expression of several different miRs between our treatment groups (Fig. 7A), it was likely that no one miR was responsible for the phenotypes we observed. Therefore, further analysis was conducted when clusters of miRs were considered to impact gene expression.

We were able to identify two miR families that were downregulated in 27HC-sEVs: let-7 and miR-129s. Both miR families have been associated with aspects of WNT signaling and stemness. To test whether decreases in sEVs delivery of these miRs influenced cancer cells, we exposed our cancer cells to DMSO-sEVs or 27HC-sEVs, followed by miR quantification in the recipient cancer cells. miR-129 expression within 4T1 and EMT6 cells was below the detection limits of our qPCR approach. In both cell lines tested, let-7 miRs were decreased in 27HC-sEVs treated cells compared to DMSO-sEVs treated ones, with the largest decreases noted in the non-adherent cells (Fig. 8).

In addition, we engineered in-house sEVs derived from neutrophils with decreased levels of all the let-7's that we identified as being downregulated after 27HC treatment. Neutrophils were treated with let-

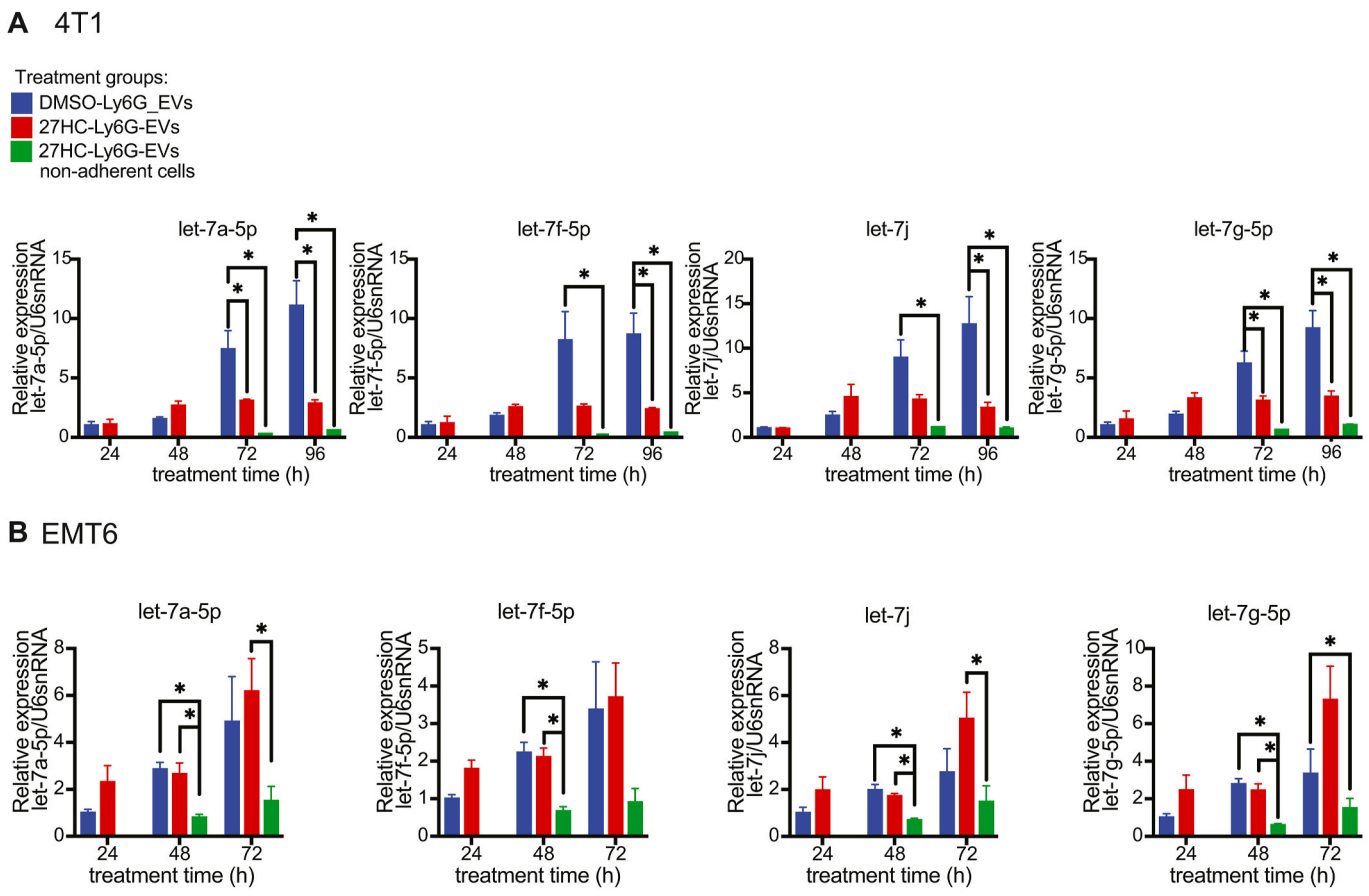

Fig. 8. Expression of *let-7* miRs *decreases in cancer cells exposed to 27HC-sEVs.* Cancer cells were exposed for indicated timepoints with sEVs harvested from neutrophils treated with either DMSO or 27HC. **(A)** Expression of different let-7 miRs through time in 4T1 cells exposed to DMSO-sEVs or 27HC-sEVs. **(B)** Expression of different let-7 miRs through time in EMT6 cells exposed to DMSO-sEVs or 27HC-sEVs. Statistical analyses were performed using one-way ANOVA followed by Tukey's multiple comparison test, N = 3/group, with an asterisk (*) denoting $P < 0.05$. All data are presented as mean ± SEM.

7a-5p, let-7f-5p, let-7g-5p, and let-7j inhibitors (antisense oligonucleotides; miRCURY LNA miRNA inhibitors), and sEVs were isolated. These sEVs were then used to treat cancer cells. First, we confirmed that let-7's inhibitors work to reduce the expression of the expected let-7 miRs in neutrophils (Fig. 9A) and sEVs (Fig. 9B). We compared the inhibitor group (let'7 inh) to the negative control for the inhibitor treatment (NC), and untreated cells and sEVs (no treatment; NT).

Gene expression analysis revealed that let-7 inhibition phenocopied that of 27HC-sEVs in recipient cells (Fig. 9C). As with 27HC-sEVs, WNT pathway genes (CTNNB1, GSKB, and TCF7) were upregulated. Moreover, cells gained a stem-like phenotype, based on downregulated ki67, and upregulated SOX2, OCT4, and NANOG. ALDH1A1 gene expression was upregulated, which was in contrast to our flow cytometry analysis of cells post-27HC-sEVs treatment (Fig. 2D). This may be due to altered post-transcriptional regulation. Regardless, our data suggest that let-7 inhibitors transfected into neutrophils resulted in sEVs that stimulated cells to gain a more epithelial stem-like phenotype, similar to 27HC-sEVs. Thus, it is likely that the let-7 miR family is the predominant executor of the effects observed in 27HC-sEV treated cancer cells with other miRs or other cargo fine-tuning responses.

To test this hypothesis more directly, we have performed a rescue experiment, where cancer cells were pre-treated for 4h with a cocktail of let-7 mimics (let-7a-5p, let-7g-5p, let-7f-5p and let-7j). Strikingly, pre-treatment of cancer cells with let-7 mimics completely ablated the effects of 27HC-sEVs, so much so that there were no detectable cells that had lost adherence (Fig. 10). mRNA analysis of adherent cells pretreated with the let-7 mimic cocktail and then exposed to 27HC-sEVs showed no changes in genes associated with WNT signaling, EMT or stemness (Fig. 10). Therefore, the mechanism by which 27HC-sEVs enhance WNT signaling, EMT, stemness and loss of adherence, relies on decreased let-7 miRs.

Overall, the let-7 family is likely a major driver of cancer cell pluripotency and stem-like phenotype, after exposure to 27HCA-sEVs. This results in cancer cells that are more migratory and resistant to chemotherapy, signatures of cells thought to cause metastatic recurrence (Fig. 11).

5. Discussion

EVs are crucial for maintaining regular cell-to-cell communication. They have been reported to play a significant role of messengers in tumor progression. It was previously reported that 27HC stimulates breast cancer metastasis in part by increasing the secretion of sEVs from neutrophils [37,53]. However, it was not known how these 27HC-derived sEVs stimulate metastasis. In this study, we have found that sEVs from 27HC-treated neutrophils impact cancer cells by promoting the loss of adherence (Fig. 1), initiating EMT and shifting cells towards a stem-like phenotype (Figs. 2 and 3). The culmination of these changes resulted in cells that were more resistant to cytotoxic chemotherapeutic drugs, doxorubicin and paclitaxel (Fig. 4). This represents a critical mechanism of resistance and serves as an emerging point for the development of novel strategies. Other studies have implicated sEVs in drug resistance, suggesting that this may be a common mechanism, and that cholesterol metabolites can regulate it [reviewed in 120–123].

We observed robust increases in WNT signaling, a predominant pathway leading to gaining stem-like phenotype by recipient cancer

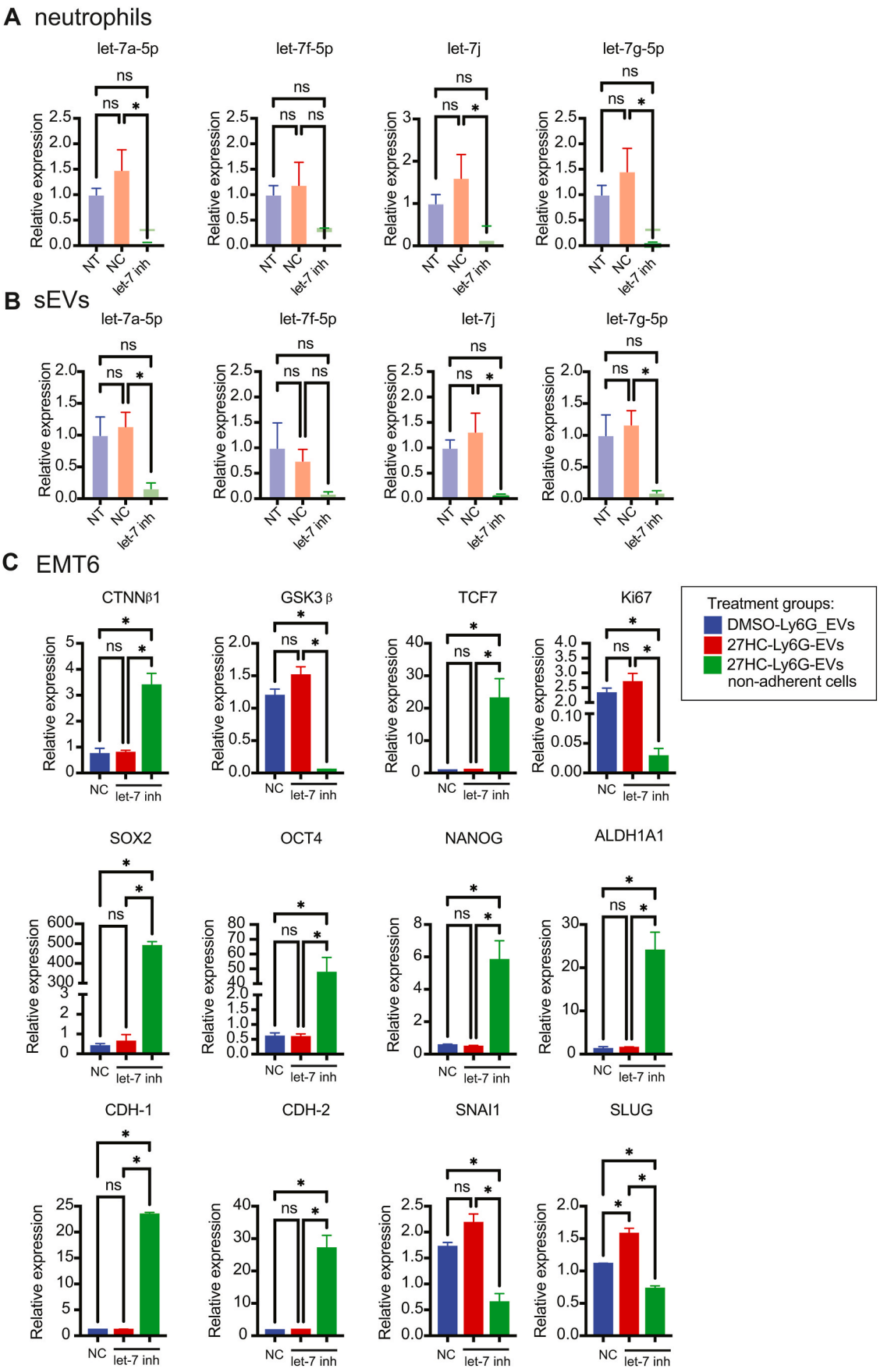

(caption on next page)

Fig. 9. ***Decreasing let-7* miRs *in sEVs results in altered expression of genes associated with the WNT pathway and stemness in recipient cancer cells, mirroring the effects of 27HC-sEVs.*** Murine neutrophils were treated with a cocktail of antisense LNA oligos (inhibitors; inh) against different let-7 miRs (let-7 inh: let-7a-5p, let-7g-5p, let7f-5p, and let7j). **(A)** RT-qPCR quantification of let-7 miR in neutrophils after treatment with let-7 inh for 48h. NT - no treated cells, NC - negative control for miR inhibitors, let-7 inh – the cocktail of 4 let-7 inhibitors in the final concentration of 5 nM. **(B)** RT-qPCR quantification of let-7 miRs in sEVs secreted from neutrophils treated with let-7 inhibitors for 48h. NT - no treated cells, NC - negative control for miR inhibitors, let-7 inh – the cocktail of 4 let-7 inhibitors in the final concentration of 5uM. **(C)** Quantification of genes associated with the WNT pathway (CTNNB1, GSK3B, and TCF7), stem cells markers (ki67, SOX2, OCT4, NANOG, and ALDH1A1) or EMT (CDH-1, CDH-2, SNAI1, and SLUG) in EMT6 cells after 72h exposure to sEVs. NC -sEVs – sEVs were isolated from neutrophils treated with negative control for miR inhibitors; let-7's inh_-sEVs. sEVs were isolated from neutrophils treated with the cocktail of 4 let-7 inhibitors at a final concentration of 5uM. Statistical analyses were performed using one-way ANOVA followed by Tukey's multiple comparison test, N = 3/group, with an asterisk (*) denoting $P < 0.05$. All data are presented as mean ± SEM.

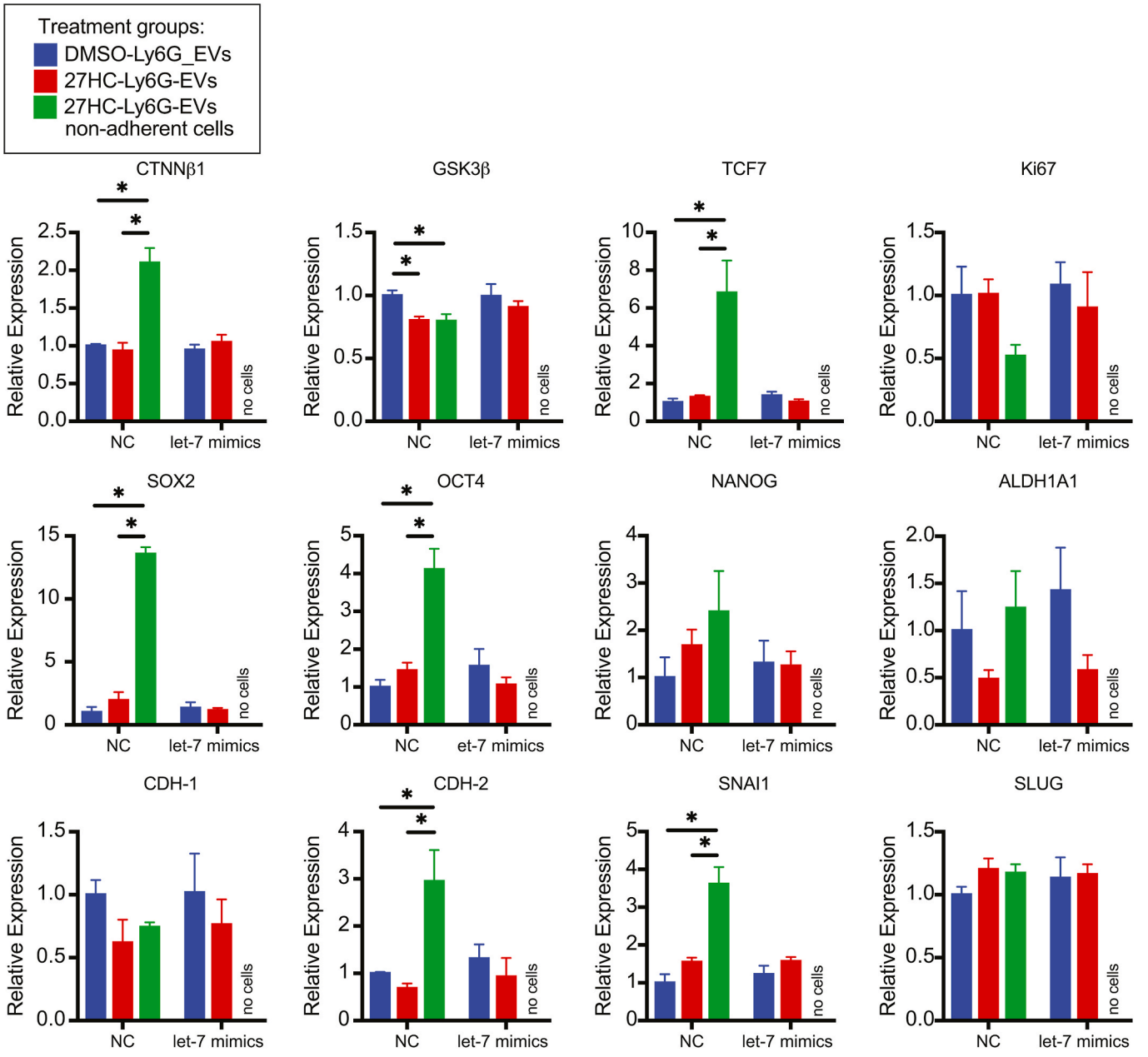

Fig. 10. ***let-7* mimics *rescue the phenotype of cancer cells treated with 27HC-sEVs.*** EMT6 cells were pre-treated with a cocktail of let-7 mimics: let-7a-5p, let-7g-5p, let7f-5p, and let7j; the final concentration being 10uM. After 4h of pre-treatment, EMT6 cells were cultured with sEVs from DMSO or 27HC treated neutrophils for an additional 48h. Quantification of genes associated with the WNT pathway (CTNNβ1, GSK3β, and TCF7), stemness (ki67, SOX2, OCT4, NANOG, and ALDH1A1) or EMT (CDH-1, CDH-2, SNAI1, and SLUG). Statistical analyses were performed using one-way ANOVA followed by Tukey's multiple comparison test, N = 3/treatment group, with an asterisk (*) denoting $P < 0.05$. All data are presented as mean ± SEM.

cells (Fig. 6 and Supplementary Fig. 10). WNT signaling has also been implicated in immunological escape [124]. When probing the mechanism behind this, we found that sEVs from 27HC-treated neutrophils lost protective let-7 miRs (Fig. 7), resulting in decreased abundance of let-7 miRs in recipient cancer cells (Fig. 8). The decreased let-7 miR expression in sEVs was due to their regulation within the parental neutrophils, suggesting that it was not through selective cargo-loading (Supplementary Fig. 14). However, the mechanisms by which 27HC

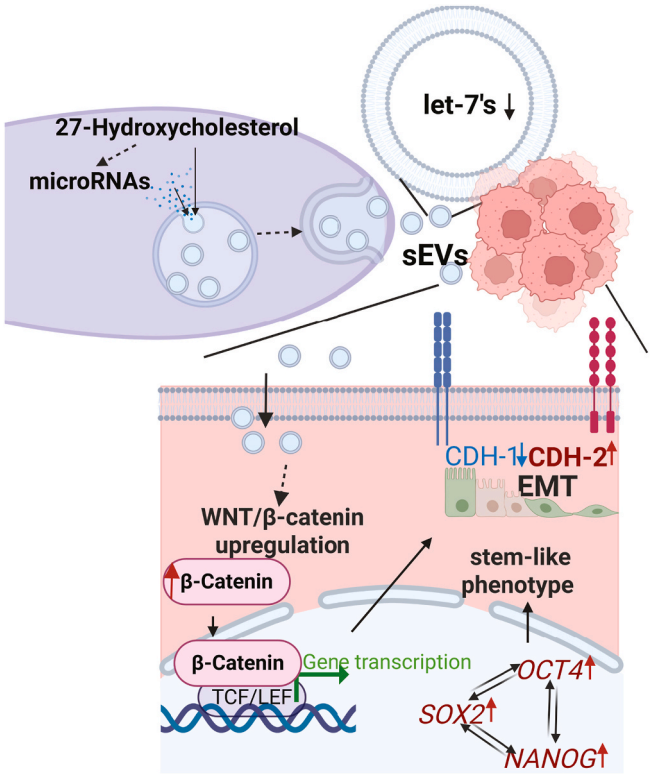

Fig. 11. ***Mechanistic overview of how EVs from neutrophils treated with 27HC result in increased EMT, stemness and loss of adherence in cancer cells.*** A proposed model whereby 27HC works in neutrophils to alter the expression of miRNAs, particularly decreasing let-7 miRs. The decreased let-7 miRs were represented in secreted EVs. The EVs are taken up by cancer cells. Normally, let-7 miRs control WNT/β-catenin signaling; a decrease in let-7 input resulting in increased WNT/β-catenin signaling, stemness and EMT. The culmination of these events leads to loss of adherence, increased migration and resistance to standard of care chemotherapies doxorubicin and paclitaxel.

modulates miRs in the neutrophil or how they are loaded into sEVs are still unknown and need to be investigated.

Our results showed that let-7 microRNA inhibition within sEVs resulted in increased loss of adherence and EMT (Fig. 9), while let-7 mimics block the induction of this phenotype by 27HC-sEVs (Fig. 10). It was still possible that 27HC-sEVs were mediating their effects by transferring 27HC itself, not just altered miR cargo. However, treatment of cancer cells with 27HC at concentrations detected in 27HC-sEVs did not result in significant changes in adherence (Supplementary Fig. 11G–H). Therefore, it most likely that the decreased let-7 microRNA in 27HC-sEVs was mediating the loss of adherence, EMT and cancer stem-like changes in recipient cancer cells (proposed model in Fig. 11).

miRs in sEVs from neutrophils inhibited the WNT pathway in recipient cancer cells, a regulatory mechanism lost in sEVs from 27HC-treated neutrophils. Consequently, cells receiving sEVs from 27HC-treated neutrophils gained a stem-like phenotype and underwent an epithelial-mesenchymal transition, the consequences of which may lead to increased metastasis and drug resistance. EMT endows cancer cells with increased motility and the ability to invade and disseminate to distant organs [96,98]. In addition, EMT is a reversible process, which can lead cancer cells to a hybrid epithelial/mesenchymal state. They can dynamically transition between those two stages, which allows them to gain properties from both phenotypes when needed [96]. Cancer stem cells can self-renew and differentiate, which contributes to tumor recurrence and heterogeneity [93,97]. Both EMT and stemness are strongly implicated in resistance to chemotherapy; in part due to their slower proliferation rate and higher expression of drug efflux pumps [103]. We found that 27HC-sEVs downregulated proliferation and promoted chemoresistance.

Understanding the dual processes of EMT and the acquisition of stemness in cancer cells is crucial for developing new therapeutic strategies to combat cancer progression, metastasis, and treatment resistance. The tumor microenvironment plays a significant role in regulating EMT and stemness. Key components driving those processes include cellular (immune cells, fibroblasts, adipocytes), signaling pathways (i.e. WNT ligands), hypoxic conditions, and extracellular matrix (ECM) remodeling [103,125]. However, little is known about how "the signal" is transduced and what exactly triggers those components that drive EMT and stemness. Here, we have found that when exposed to 27HC, neutrophils change their miR content and consequently release sEVs ("the signal") with modulated molecular cargo. Those sEVs are taken by cancer cells and sensitize the WNT signaling pathway that is a known initiator of stemness [89,105–109,115].

Targeting the 27HC pathway could offer a novel therapeutic approach in breast cancer patients [13]. Since 27HC influences the tumor and metastatic microenvironment by recruiting neutrophils and modulating sEV cargo, therapies that inhibit neutrophil recruitment, modulate sEVs release, or uptake by cancer cells might reduce the pro-tumorigenic effects of 27HC. In addition, developing compounds that specifically block 27HC's interaction with its receptors in neutrophils would decrease its ability to modulate sEVs cargo to promote cancer cell metastasis [17,19,39]. WNT/β-catenin signaling has been implicated in breast cancer pathophysiology [126]. It has been implicated in stemness and drug resistance [127]. However, due to its requirement in normal tissue physiology, including intestinal stem cell renewal, it has been very challenging to target therapeutically [128]. To reduce undesirable side effects, there are now attempts to disrupt WNT signaling at different levels in its signal transduction cascade, although these approaches are not in the clinic yet. Interestingly, membrane cholesterol can activate WNT signaling through direct interactions with DVL, providing an alternative avenue for drug development [129]. Therefore, combining 27HC pathway modulators, neutrophil recruitment inhibitors, and sEV-release modulators with existing breast cancer treatments, may represent improved ways to target WNT signaling in breast cancer with reduced side effects.

It is important to note that in addition to modulating EV biogenesis and cargo, 27HC or other cholesterol metabolites may influence other neutrophil functions. These include migration, phagocytosis, degranulation, and NETosis [130]. NETosis, the extrusion of DNA and associated proteins to form extracellular NETs [131]. NETosis has recently been implicated in breast cancer progression [73,132–134]. Indeed, we have previously shown that 27HC-treated neutrophils suppress T cell expansion [34]. Future work will have to address how oxysterols such as 27HC may regulate these other neutrophil functions.

Collectively, our results indicate that 27HC modulates miR levels in neutrophils, leading to the release of sEVs with modified miRs that are taken up by cancer cells (Fig. 11). This ultimately results in the upregulation of genes connected to WNT and stemness. Consequently, cancer cells lose their adherence in an EMT process, gaining migratory, stem-like phenotype, and chemoresistance.

CRediT authorship contribution statement

Natalia Krawczynska: Writing – review & editing, Writing – original draft, Supervision, Resources, Project administration, Methodology, Investigation, Funding acquisition, Formal analysis, Data curation, Conceptualization. **Yu Wang:** Writing – review & editing, Writing – original draft, Methodology, Investigation, Formal analysis, Data curation, Conceptualization. **Ki Lim:** Investigation. **Anasuya Das Gupta:** Writing – review & editing, Writing – original draft, Supervision, Methodology, Investigation, Formal analysis, Data curation, Conceptualization. **Ralph John Emerson J. Molino:** Writing – review & editing, Writing – original draft, Methodology, Investigation, Formal analysis, Data curation, Conceptualization. **Adam Lenczowski:** Investigation.

Marwan Abughazaleh: Investigation. **Shruti V. Bendre:** Writing – review & editing, Writing – original draft, Methodology, Investigation, Conceptualization. **Yifan Fei:** Writing – review & editing, Writing – original draft, Methodology, Investigation. **Hannah Kim:** Methodology, Investigation. **Lara I. Kockaya:** Methodology, Investigation. **Claire P. Schane:** Writing – review & editing, Writing – original draft, Methodology, Investigation. **Dhanya Pradeep:** Writing – review & editing, Investigation. **Desirée Rodriguez-Casiano:** Writing – review & editing, Methodology, Investigation. **Alvaro G. Hernandez:** Writing – review & editing, Methodology, Investigation. **Jenny Drnevich:** Writing – review & editing, Writing – original draft, Methodology, Investigation. **Jefferson Chan:** Writing – review & editing, Writing – original draft, Resources. **Lawrence W. Dobrucki:** Writing – review & editing, Writing – original draft, Resources, Methodology, Conceptualization. **Marni D. Boppart:** Writing – review & editing, Writing – original draft, Supervision, Methodology, Investigation. **Stephanie M. Cologna:** Writing – review & editing, Writing – original draft, Supervision, Methodology, Investigation, Conceptualization. **Julie Ostrander:** Writing – review & editing, Writing – original draft, Supervision, Resources, Methodology. **Erik R. Nelson:** Writing – review & editing, Writing – original draft, Supervision, Resources, Project administration, Methodology, Investigation, Funding acquisition, Formal analysis, Data curation, Conceptualization.

Funding information

Department of Defense Era of Hope Scholar Award BC200206/W81XWH-20-BCRP-EOHS (ERN)

Cancer Center at Illinois, University of Illinois Urbana Champaign (ERN)

National Institutes of Health grants R01CA234025 and R01CA288207 (ERN)

Postdoctoral Fellows Program at the Beckman Institute for Advanced Science and Technology (NK), Illinois Postbaccalaureate Research Program (DRC)

TiME Fellowship Award NIH T32EB019944 (CPS)

National Science Foundation CAREER Award #214920 (SMC)

Declaration of competing interest

The authors do not have anything to disclose or conflicts of interest that would influence the results or interpretation within this manuscript.

Acknowledgments

The Cancer Center at Illinois Tumor Engineering and Phenotyping Shared Resource (TEP) provided certain cell lines and routine mycoplasma testing (directed and assisted by Hui Xu and Huimin Zhang). We would like to thank Chris Wright, an Associate Director of DNA Services at Roy J. Carver Biotechnology Center University of Illinois at Urbana-Champaign for her contribution to the experiment design and best practices for the sequencing experiments. A version of this manuscript is available as a preprint: bioRxiv 2024.08.02.606061; doi: https://doi.org/10.1101/2024.08.02.606061.

Appendix A. Supplementary data

Supplementary data to this article can be found online at https://doi.org/10.1016/j.canlet.2025.218105.

Data availability

Sequencing data has been deposited to GEO [GSE272477 and GSE272476].

References

[1] A.N. Giaquinto, H. Sung, K.D. Miller, J.L. Kramer, L.A. Newman, A. Minihan, A. Jemal, R.L. Siegel, Breast cancer statistics, CA Cancer J. Clin. 72 (2022) 524–541, 2022.

[2] F. Kamangar, G.M. Dores, W.F. Anderson, Patterns of cancer incidence, mortality, and prevalence across five continents: defining priorities to reduce cancer disparities in different geographic regions of the world, J. Clin. Oncol. 24 (2006) 2137–2150.

[3] G.J. Morris, S. Naidu, A.K. Topham, F. Guiles, Y. Xu, P. McCue, G.F. Schwartz, P. K. Park, A.L. Rosenberg, K. Brill, E.P. Mitchell, Differences in breast carcinoma characteristics in newly diagnosed African-American and Caucasian patients: a single-institution compilation compared with the National Cancer Institute's Surveillance, Epidemiology, and end results database, Cancer 110 (2007) 876–884.

[4] P. Kumar, R. Aggarwal, An overview of triple-negative breast cancer, Arch. Gynecol. Obstet. 293 (2016) 247–269.

[5] F. Borri, A. Granaglia, Pathology of triple negative breast cancer, Semin. Cancer Biol. 72 (2021) 136–145.

[6] L. Yin, J.J. Duan, X.W. Bian, S.C. Yu, Triple-negative breast cancer molecular subtyping and treatment progress, Breast Cancer Res. 22 (2020) 61.

[7] P. Schmid, H.S. Rugo, S. Adams, A. Schneeweiss, C.H. Barrios, H. Iwata, V. Dieras, V. Henschel, L. Molinero, S.Y. Chui, V. Maiya, A. Husain, E.P. Winer, S. Loi, L. A. Emens, I.M. Investigators, Atezolizumab plus nab-paclitaxel as first-line treatment for unresectable, locally advanced or metastatic triple-negative breast cancer (IMpassion130): updated efficacy results from a randomised, double-blind, placebo-controlled, phase 3 trial, Lancet Oncol. 21 (2020) 44–59.

[8] N.V. Desai, A.R. Tan, Targeted therapies and the evolving standard of care for triple-negative and germline BRCA1/2-Mutated breast cancers in the High-Risk, early-stage setting, JCO Precis Oncol 7 (2023) e2200446.

[9] M.E. Robson, S.A. Im, E. Senkus, B. Xu, S.M. Domchek, N. Masuda, S. Delaloge, N. Tung, A. Armstrong, M. Dymond, A. Fielding, A. Allen, P. Conte, OlympiAD extended follow-up for overall survival and safety: olaparib versus chemotherapy treatment of physician's choice in patients with a germline BRCA mutation and HER2-negative metastatic breast cancer, Eur. J. Cancer 184 (2023) 39–47.

[10] B. Huang, B.L. Song, C. Xu, Cholesterol metabolism in cancer: mechanisms and therapeutic opportunities, Nat. Metab. 2 (2020) 132–141.

[11] L. Ma, W. Cho, E.R. Nelson, Our evolving understanding of how 27-hydroxycholesterol influences cancer, Biochem. Pharmacol. 196 (2022) 114621.

[12] A.E. Baek, E.R. Nelson, The contribution of cholesterol and its metabolites to the pathophysiology of breast cancer, Horm Cancer 7 (2016) 219–228.

[13] C. Le Cornet, B. Walter, D. Sookthai, T.S. Johnson, T. Kuhn, E. Herpel, R. Kaaks, R.T. Fortner, Circulating 27-hydroxycholesterol and breast cancer tissue expression of CYP27A1, CYP7B1, LXR-beta, and ERbeta: results from the EPIC-Heidelberg cohort, Breast Cancer Res. 22 (2020) 23.

[14] I.H.K. Dias, I. Milic, C. Heiss, O.S. Ademowo, M.C. Polidori, A. Devitt, H. R. Griffiths, Inflammation, lipid (Per)oxidation, and redox regulation, Antioxid Redox Signal 33 (2020) 166–190.

[15] C.D. DuSell, M. Umetani, P.W. Shaul, D.J. Mangelsdorf, D.P. McDonnell, 27-hydroxycholesterol is an endogenous selective estrogen receptor modulator, Mol. Endocrinol. 22 (2008) 65–77.

[16] M. Umetani, H. Domoto, A.K. Gormley, I.S. Yuhanna, C.L. Cummins, N.B. Javitt, K.S. Korach, P.W. Shaul, D.J. Mangelsdorf, 27-Hydroxycholesterol is an endogenous SERM that inhibits the cardiovascular effects of estrogen, Nat Med 13 (2007) 1185–1192.

[17] E.R. Nelson, S.E. Wardell, J.S. Jasper, S. Park, S. Suchindran, M.K. Howe, N. J. Carver, R.V. Pillai, P.M. Sullivan, V. Sondhi, M. Umetani, J. Geradts, D. P. McDonnell, 27-Hydroxycholesterol links hypercholesterolemia and breast cancer pathophysiology, Science 342 (2013) 1094–1098.

[18] Q. Wu, T. Ishikawa, R. Sirianni, H. Tang, J.G. McDonald, I.S. Yuhanna, B. Thompson, L. Girard, C. Mineo, R.A. Brekken, M. Umetani, D.M. Euhus, Y. Xie, P.W. Shaul, 27-Hydroxycholesterol promotes cell-autonomous, ER-positive breast cancer growth, Cell Rep. 5 (2013) 637–645.

[19] A.E. Baek, Y.A. Yu, S. He, S.E. Wardell, C.Y. Chang, S. Kwon, R.V. Pillai, H. B. McDowell, J.W. Thompson, L.G. Dubois, P.M. Sullivan, J.K. Kemper, M. D. Gunn, D.P. McDonnell, E.R. Nelson, The cholesterol metabolite 27 hydroxycholesterol facilitates breast cancer metastasis through its actions on immune cells, Nat. Commun. 8 (2017) 864.

[20] K. Undela, V. Srikanth, D. Bansal, Statin use and risk of breast cancer: a meta-analysis of observational studies, Breast Cancer Res. Treat. 135 (2012) 261–269.

[21] C. Danilo, P.G. Frank, Cholesterol and breast cancer development, Curr. Opin. Pharmacol. 12 (2012) 677–682.

[22] M. Bahl, M. Ennis, I.F. Tannock, J.E. Hux, K.I. Pritchard, J. Koo, P.J. Goodwin, Serum lipids and outcome of early-stage breast cancer: results of a prospective cohort study, Breast Cancer Res. Treat. 94 (2005) 135–144.

[23] T.P. Ahern, L. Pedersen, M. Tarp, D.P. Cronin-Fenton, J.P. Garne, R.A. Silliman, H.T. Sorensen, T.L. Lash, Statin prescriptions and breast cancer recurrence risk: a Danish nationwide prospective cohort study, Journal of the National Cancer Institute 103 (2011) 1461–1468.

[24] M.L. Kwan, L.A. Habel, E.D. Flick, C.P. Quesenberry, B. Caan, Post-diagnosis statin use and breast cancer recurrence in a prospective cohort study of early stage breast cancer survivors, Breast Cancer Res. Treat. 109 (2008) 573–579.

[25] S.F. Nielsen, B.G. Nordestgaard, S.E. Bojesen, Statin use and reduced cancer-related mortality, N. Engl. J. Med. 367 (2012) 1792–1802.

[26] M.O. Murto, N. Simolin, O. Arponen, A. Siltari, M. Artama, K. Visvanathan, A. Jukkola, T.J. Murtola, Statin use, cholesterol level, and mortality among females with breast cancer, JAMA Netw. Open 6 (2023) e2343861.
[27] M.K. Nowakowska, X. Lei, M.T. Thompson, S.F. Shaitelman, M.R. Wehner, W. A. Woodward, S.H. Giordano, K.T. Nead, Association of statin use with clinical outcomes in patients with triple-negative breast cancer, Cancer (2021).
[28] S.F. Shaitelman, M.C. Stauder, P. Allen, S. Reddy, S. Lakoski, B. Atkinson, J. Reddy, D. Amaya, W. Guerra, N. Ueno, A. Caudle, W. Tereffe, W.A. Woodward, Impact of Statin use on outcomes in triple negative breast cancer, J. Cancer 8 (2017) 2026–2032.
[29] S. Borgquist, A. Giobbie-Hurder, T.P. Ahern, J.E. Garber, M. Colleoni, I. Lang, M. Debled, B. Ejlertsen, R. von Moos, I. Smith, A.S. Coates, A. Goldhirsch, M. Rabaglio, K.N. Price, R.D. Gelber, M.M. Regan, B. Thurlimann, Cholesterol, cholesterol-lowering medication use, and breast cancer outcome in the BIG 1-98 Study, J. Clin. Oncol. 35 (2017) 1179–1188.
[30] D.L. Lu, C. Le Cornet, D. Sookthai, T.S. Johnson, R. Kaaks, R.T. Fortner, Circulating 27-Hydroxycholesterol and breast cancer risk: results from the EPIC-Heidelberg cohort, Journal of the National Cancer Institute 111 (2019) 365–371.
[31] M.C. DeRouen, J. Yang, Y. Li, A.A. Franke, A.N. Tome, K.K. White, B. Y. Hernandez, Y. Shvetsov, V. Setiawan, A.H. Wu, L.R. Wilkens, L. Le Marchand, L.W.M. Loo, I. Cheng, Circulating 27-hydroxycholesterol, lipids, and steroid hormones in breast cancer risk: a nested case-control study of the Multiethnic Cohort Study, Breast Cancer Res. 25 (2023) 95.
[32] N.S. Decker, T. Johnson, S. Behrens, N. Obi, R. Kaaks, J. Chang-Claude, R. T. Fortner, Endogenous estrogen receptor modulating oxysterols and breast cancer prognosis: results from the MARIE patient cohort, Br. J. Cancer 129 (2023) 492–502.
[33] S. He, L. Ma, A.E. Baek, A. Vardanyan, V. Vembar, J.J. Chen, A.T. Nelson, J. E. Burdette, E.R. Nelson, Host CYP27A1 expression is essential for ovarian cancer progression, Endocr. Relat. Cancer 26 (2019) 659–675.
[34] L. Ma, L. Wang, A.T. Nelson, C. Han, S. He, M.A. Henn, K. Menon, J.J. Chen, A. E. Baek, A. Vardanyan, S.H. Shahoei, S. Park, D.J. Shapiro, S.G. Nanjappa, E. R. Nelson, 27-Hydroxycholesterol acts on myeloid immune cells to induce T cell dysfunction, promoting breast cancer progression, Cancer letters 493 (2020) 266–283.
[35] E.R. Nelson, The significance of cholesterol and its metabolite, 27-hydroxycholesterol in breast cancer, Mol. Cell. Endocrinol. 466 (2018) 73–80.
[36] Y. Wang, S.V. Bendre, S.A. Krauklis, A.J. Steelman, E.R. Nelson, Role of protein regulators of cholesterol homeostasis in immune modulation and cancer pathophysiology, Endocrinology 166 (2025).
[37] A.E. Baek, Y.-R.A. Yu, S. He, S.E. Wardell, C.-Y. Chang, S. Kwon, R.V. Pillai, H. B. McDowell, J.W. Thompson, L.G. Dubois, P.M. Sullivan, J.K. Kemper, M. D. Gunn, D.P. McDonnell, E.R. Nelson, The cholesterol metabolite 27 hydroxycholesterol facilitates breast cancer metastasis through its actions on immune cells, Nat. Commun. 8 (2017) 864.
[38] A.W. Lambert, D.R. Pattabiraman, R.A. Weinberg, Emerging biological principles of metastasis, Cell 168 (2017) 670–691.
[39] L. Ma, H.E. Vidana Gamage, S. Tiwari, C. Han, M.A. Henn, N. Krawczynska, P. Dibaeinia, G.J. Koelwyn, A. Das Gupta, R.O. Bautista Rivas, C.L. Wright, F. Xu, K.J. Moore, S. Sinha, E.R. Nelson, The liver X receptor is selectively modulated to differentially alter female mammary metastasis-associated Myeloid cells, Endocrinology 163 (2022).
[40] N. Aceto, A. Bardia, D.T. Miyamoto, M.C. Donaldson, B.S. Wittner, J.A. Spencer, M. Yu, A. Pely, A. Engstrom, H. Zhu, B.W. Brannigan, R. Kapur, S.L. Stott, T. Shioda, S. Ramaswamy, D.T. Ting, C.P. Lin, M. Toner, D.A. Haber, S. Maheswaran, Circulating tumor cell clusters are oligoclonal precursors of breast cancer metastasis, Cell 158 (2014) 1110–1122.
[41] N. Aceto, M. Toner, S. Maheswaran, D.A. Haber, En Route to Metastasis: circulating Tumor Cell Clusters and Epithelial-to-Mesenchymal Transition, Trends Cancer 1 (2015) 44–52.
[42] P.F. Yu, Y. Huang, Y.Y. Han, L.Y. Lin, W.H. Sun, A.B. Rabson, Y. Wang, Y.F. Shi, TNFalpha-activated mesenchymal stromal cells promote breast cancer metastasis by recruiting CXCR2(+) neutrophils, Oncogene 36 (2017) 482–490.
[43] K. Zhu, P. Li, Y. Mo, J. Wang, X. Jiang, J. Ge, W. Huang, Y. Liu, Y. Tang, Z. Gong, Q. Liao, X. Li, G. Li, W. Xiong, Z. Zeng, J. Yu, Neutrophils: accomplices in metastasis, Cancer Lett. 492 (2020) 11–20.
[44] S.K. Wculek, I. Malanchi, Neutrophils support lung colonization of metastasis-initiating breast cancer cells, Nature 528 (2015) 413–417.
[45] Z. Wang, C. Yang, L. Li, Z. Zhang, J. Pan, K. Su, W. Chen, J. Li, F. Qiu, J. Huang, CD62L(dim) neutrophils specifically migrate to the lung and participate in the Formation of the pre-metastatic niche of breast cancer, Front. Oncol. 10 (2020) 540484.
[46] E. Hawila, H. Razon, G. Wildbaum, C. Blattner, Y. Sapir, Y. Shaked, V. Umansky, N. Karin, CCR5 directs the mobilization of CD11b(+)Gr1(+)Ly6C(low) polymorphonuclear Myeloid cells from the bone marrow to the blood to support tumor development, Cell Rep. 21 (2017) 2212–2222.
[47] S.B. Coffelt, K. Kersten, C.W. Doornebal, J. Weiden, K. Vrijland, C.S. Hau, N.J. M. Verstegen, M. Ciampricotti, L. Hawinkels, J. Jonkers, K.E. de Visser, IL-17-producing gammadelta T cells and neutrophils conspire to promote breast cancer metastasis, Nature 522 (2015) 345–348.
[48] D.F. Quail, O.C. Olson, P. Bhardwaj, L.A. Walsh, L. Akkari, M.L. Quick, I.C. Chen, N. Wendel, N. Ben-Chetrit, J. Walker, P.R. Holt, A.J. Dannenberg, J.A. Joyce, Obesity alters the lung myeloid cell landscape to enhance breast cancer metastasis through IL5 and GM-CSF, Nat. Cell Biol. 19 (2017) 974–987.
[49] M. Wu, M. Ma, Z. Tan, H. Zheng, X. Liu, Neutrophil: a new player in metastatic cancers, Front. Immunol. 11 (2020) 565165.
[50] M.T. Masucci, M. Minopoli, M.V. Carriero, Tumor associated neutrophils. Their role in tumorigenesis, metastasis, prognosis and therapy, Front. Oncol. 9 (2019) 1146.
[51] E. Uribe-Querol, C. Rosales, Neutrophils in cancer: two sides of the same coin, J Immunol Res 2015 (2015) 983698.
[52] A.D. Gregory, A.M. Houghton, Tumor-associated neutrophils: new targets for cancer therapy, Cancer Res. 71 (2011) 2411–2416.
[53] A.E. Baek, N. Krawczynska, A. Das Gupta, S.V. Dvoretskiy, S. You, J. Park, Y. H. Deng, J.E. Sorrells, B.P. Smith, L. Ma, A.T. Nelson, H.B. McDowell, A. Sprenger, M.A. Henn, Z. Madak-Erdogan, H. Kong, S.A. Boppart, M.D. Boppart, E.R. Nelson, The cholesterol metabolite 27-hydroxycholesterol increases the secretion of extracellular vesicles which promote breast cancer progression, Endocrinology (2021).
[54] A. Das Gupta, J. Park, J.E. Sorrells, H. Kim, N. Krawczynska, D. Pradeep, Y. Wang, H.E. Vidana Gamage, A.T. Nelczyk, S.A. Boppart, M.D. Boppart, E.R. Nelson, 27-Hydroxycholesterol enhances secretion of extracellular vesicles by ROS-Induced dysregulation of lysosomes, Endocrinology (2024).
[55] A. Das Gupta, N. Krawczynska, E.R. Nelson, Extracellular vesicles-the next frontier in endocrinology, Endocrinology 162 (2021).
[56] W. Liang, S. Sagar, R. Ravindran, R.H. Najor, J.M. Quiles, L. Chi, R.Y. Diao, B. P. Woodall, L.J. Leon, E. Zumaya, J. Duran, D.M. Cauvi, A. De Maio, E.D. Adler, A.B. Gustafsson, Mitochondria are secreted in extracellular vesicles when lysosomal function is impaired, Nat. Commun. 14 (2023) 5031.
[57] F. Kolonics, V. Szeifert, C.I. Timar, E. Ligeti, A.M. Lorincz, The functional heterogeneity of neutrophil-derived extracellular vesicles reflects the status of the parent cell, Cells 9 (2020).
[58] D.S. Rubenich, N. Omizzollo, M.J. Szczepanski, T.E. Reichert, T.L. Whiteside, N. Ludwig, E. Braganhol, Small extracellular vesicle-mediated bidirectional crosstalk between neutrophils and tumor cells, Cytokine Growth Factor Rev. 61 (2021) 16–26.
[59] A. Tyagi, S.Y. Wu, S. Sharma, K. Wu, D. Zhao, R. Deshpande, R. Singh, W. Li, U. Topaloglu, J. Ruiz, K. Watabe, Exosomal miR-4466 from nicotine-activated neutrophils promotes tumor cell stemness and metabolism in lung cancer metastasis, Oncogene 41 (2022) 3079–3092.
[60] A. Tyagi, S. Sharma, K. Wu, S.Y. Wu, F. Xing, Y. Liu, D. Zhao, R.P. Deshpande, R. B. D'Agostino Jr., K. Watabe, Nicotine promotes breast cancer metastasis by stimulating N2 neutrophils and generating pre-metastatic niche in lung, Nat. Commun. 12 (2021) 474.
[61] A.S. Chao, P. Matak, K. Pegram, J. Powers, C. Hutson, R. Jo, L. Dubois, J. W. Thompson, P.B. Smith, V. Jain, C. Liu, N.E. Younge, B. Rikard, E.Y. Reyes, M. L. Shinohara, S.G. Gregory, R.N. Goldberg, E.J. Benner, 20-alphaHydroxycholesterol, an oxysterol in human breast milk, reverses mouse neonatal white matter injury through Gli-dependent oligodendrogenesis, Cell Stem Cell 30 (2023) 1054–1071 e1058.
[62] G.-H. Zhao, Z.-X. Wu, M. Zhang, Y. Luo, D.-Y. Zhou, A sensitive UHPLC-electrospray tandem mass spectrometry method for the simultaneous quantification of 8 oxysterols and cholesterol in oysters (Crassostrea gigas) with different thermal cooking procedures, J. Food Compos. Anal. 138 (2025) 107025.
[63] P.A. Ewels, A. Peltzer, S. Fillinger, H. Patel, J. Alneberg, A. Wilm, M.U. Garcia, P. Di Tommaso, S. Nahnsen, The nf-core framework for community-curated bioinformatics pipelines, Nat. Biotechnol. 38 (2020) 276–278.
[64] A. Kozomara, S. Griffiths-Jones, miRBase: annotating high confidence microRNAs using deep sequencing data, Nucleic Acids Res. 42 (2014) D68–D73.
[65] A. Frankish, M. Diekhans, I. Jungreis, J. Lagarde, J.E. Loveland, J.M. Mudge, C. Sisu, J.C. Wright, J. Armstrong, I. Barnes, A. Berry, A. Bignell, C. Boix, S. Carbonell Sala, F. Cunningham, T. Di Domenico, S. Donaldson, I.T. Fiddes, C. Garcia Giron, J.M. Gonzalez, T. Grego, M. Hardy, T. Hourlier, K.L. Howe, T. Hunt, O.G. Izuogu, R. Johnson, F.J. Martin, L. Martinez, S. Mohanan, P. Muir, F.C.P. Navarro, A. Parker, B. Pei, F. Pozo, F.C. Riera, M. Ruffier, B.M. Schmitt, E. Stapleton, M.M. Suner, I. Sycheva, B. Uszczynska-Ratajczak, M.Y. Wolf, J. Xu, Y.T. Yang, A. Yates, D. Zerbino, Y. Zhang, J.S. Choudhary, M. Gerstein, R. Guigo, T.J.P. Hubbard, M. Kellis, B. Paten, M.L. Tress, P. Flicek, Gencode 2021, Nucleic Acids Res. 49 (2021) D916–D923.
[66] P. Di Tommaso, M. Chatzou, E.W. Floden, P.P. Barja, E. Palumbo, C. Notredame, Nextflow enables reproducible computational workflows, Nat. Biotechnol. 35 (2017) 316–319.
[67] M.D. Robinson, A. Oshlack, A scaling normalization method for differential expression analysis of RNA-seq data, Genome Biol. 11 (2010) R25.
[68] M.D. Robinson, D.J. McCarthy, G.K. Smyth, edgeR: a Bioconductor package for differential expression analysis of digital gene expression data, Bioinformatics 26 (2010) 139–140.
[69] S. Liu, Z. Wang, R. Zhu, F. Wang, Y. Cheng, Y. Liu, Three differential expression analysis methods for RNA sequencing: limma, EdgeR, DESeq2, J. Vis. Exp. (2021).
[70] C. Anorma, J. Hedhli, T.E. Bearrood, N.W. Pino, S.H. Gardner, H. Inaba, P. Zhang, Y. Li, D. Feng, S.E. Dibrell, K.A. Kilian, L.W. Dobrucki, T.M. Fan, J. Chan, Surveillance of cancer stem cell plasticity using an isoform-selective fluorescent probe for aldehyde dehydrogenase 1A1, ACS Cent. Sci. 4 (2018) 1045–1055.
[71] T.H. Truong, E.A. Benner, K.M. Hagen, N.A. Temiz, C.P. Kerkvliet, Y. Wang, E. Cortes-Sanchez, C.H. Yang, M.C. Trousdell, T. Pengo, K.P. Guillen, B.E. Welm, C.O. Dos Santos, S. Telang, C.A. Lange, J.H. Ostrander, PELP1/SRC-3-dependent regulation of metabolic PFKFB kinases drives therapy resistant ER(+) breast cancer, Oncogene 40 (2021) 4384–4397.
[72] C.A. Schneider, W.S. Rasband, K.W. Eliceiri, NIH Image to ImageJ: 25 years of image analysis, Nat. Methods 9 (2012) 671–675.
[73] J. Albrengues, M.A. Shields, D. Ng, C.G. Park, A. Ambrico, M.E. Poindexter, P. Upadhyay, D.L. Uyeminami, A. Pommier, V. Kuttner, E. Bruzas, L. Maiorino,

C. Bautista, E.M. Carmona, P.A. Gimotty, D.T. Fearon, K. Chang, S.K. Lyons, K. E. Pinkerton, L.C. Trotman, M.S. Goldberg, J.T. Yeh, M. Egeblad, Neutrophil extracellular traps produced during inflammation awaken dormant cancer cells in mice, Science 361 (2018).
[74] P. Ewels, M. Magnusson, S. Lundin, M. Kaller, MultiQC: summarize analysis results for multiple tools and samples in a single report, Bioinformatics 32 (2016) 3047–3048.
[75] R. Patro, G. Duggal, M.I. Love, R.A. Irizarry, C. Kingsford, Salmon provides fast and bias-aware quantification of transcript expression, Nat. Methods 14 (2017) 417–419.
[76] C. Soneson, M.I. Love, M.D. Robinson, Differential analyses for RNA-seq: transcript-level estimates improve gene-level inferences, F1000Res 4 (2015) 1521.
[77] M.E. Ritchie, B. Phipson, D. Wu, Y. Hu, C.W. Law, W. Shi, G.K. Smyth, Limma powers differential expression analyses for RNA-sequencing and microarray studies, Nucleic Acids Res. 43 (2015) e47.
[78] C.W. Law, Y. Chen, W. Shi, G.K. Smyth, Voom: precision weights unlock linear model analysis tools for RNA-seq read counts, Genome Biol. 15 (2014) R29.
[79] B. Zhang, S. Horvath, A general framework for weighted gene co-expression network analysis, Stat. Appl. Genet. Mol. Biol. 4 (2005). Article17.
[80] P. Langfelder, S. Horvath, WGCNA: an R package for weighted correlation network analysis, BMC Bioinf. 9 (2008) 559.
[81] S.X. Ge, D. Jung, R. Yao, ShinyGO: a graphical gene-set enrichment tool for animals and plants, Bioinformatics 36 (2020) 2628–2629.
[82] M. Record, M. Attia, K. Carayon, L. Pucheu, J. Bunay, R. Soules, S. Ayadi, B. Payre, L. Perrin-Cocon, F. Bourgailh, A. Lamaziere, V. Lotteau, M. Poirot, S. Silvente-Poirot, P. de Medina, Targeting the liver X receptor with dendrogenin A differentiates tumour cells to secrete immunogenic exosome-enriched vesicles, J. Extracell. Vesicles 11 (2022) e12211.
[83] D.L. Dexter, H.M. Kowalski, B.A. Blazar, Z. Fligiel, R. Vogel, G.H. Heppner, Heterogeneity of tumor cells from a single mouse mammary tumor, Cancer Res. 38 (1978) 3174–3181.
[84] S.C. Rockwell, R.F. Kallman, L.F. Fajardo, Characteristics of a serially transplanted mouse mammary tumor and its tissue-culture-adapted derivative, J Natl Cancer Inst 49 (1972) 735–749.
[85] D.S. Micalizzi, S. Maheswaran, D.A. Haber, A conduit to metastasis: circulating tumor cell biology, Genes Dev. 31 (2017) 1827–1840.
[86] A. Liu, X. Yu, S. Liu, Pluripotency transcription factors and cancer stem cells: small genes make a big difference, Chin. J. Cancer 32 (2013) 483–487.
[87] M.L. De Angelis, F. Francescangeli, A. Zeuner, Breast cancer stem cells as drivers of tumor chemoresistance, dormancy and relapse: new challenges and therapeutic opportunities, Cancers (Basel) (2019) 11.
[88] X. Zhang, K. Powell, L. Li, Breast cancer stem cells: biomarkers, identification and isolation methods, regulating mechanisms, cellular origin, and beyond, Cancers (Basel) 12 (2020).
[89] J. Dittmer, Breast cancer stem cells: features, key drivers and treatment options, Semin. Cancer Biol. 53 (2018) 59–74.
[90] M. Al-Hajj, M.S. Wicha, A. Benito-Hernandez, S.J. Morrison, M.F. Clarke, Prospective identification of tumorigenic breast cancer cells, Proc. Natl. Acad. Sci. U. S. A. 100 (2003) 3983–3988.
[91] C. Sheridan, H. Kishimoto, R.K. Fuchs, S. Mehrotra, P. Bhat-Nakshatri, C. H. Turner, R. Goulet Jr., S. Badve, H. Nakshatri, CD44+/CD24- breast cancer cells exhibit enhanced invasive properties: an early step necessary for metastasis, Breast Cancer Res. 8 (2006) R59.
[92] Y. Yan, X. Zuo, D. Wei, Concise review: emerging role of CD44 in cancer stem cells: a promising biomarker and therapeutic target, Stem Cells Transl. Med. 4 (2015) 1033–1043.
[93] S.Q. Geng, A.T. Alexandrou, J.J. Li, Breast cancer stem cells: multiple capacities in tumor metastasis, Cancer Lett. 349 (2014) 1–7.
[94] C. Ginestier, M.H. Hur, E. Charafe-Jauffret, F. Monville, J. Dutcher, M. Brown, J. Jacquemier, P. Viens, C.G. Kleer, S. Liu, A. Schott, D. Hayes, D. Birnbaum, M. S. Wicha, G. Dontu, ALDH1 is a marker of normal and malignant human mammary stem cells and a predictor of poor clinical outcome, Cell Stem Cell 1 (2007) 555–567.
[95] H. Tomita, K. Tanaka, T. Tanaka, A. Hara, Aldehyde dehydrogenase 1A1 in stem cells and cancer, Oncotarget 7 (2016) 11018–11032.
[96] S. Liu, Y. Cong, D. Wang, Y. Sun, L. Deng, Y. Liu, R. Martin-Trevino, L. Shang, S. P. McDermott, M.D. Landis, S. Hong, A. Adams, R. D'Angelo, C. Ginestier, E. Charafe-Jauffret, S.G. Clouthier, D. Birnbaum, S.T. Wong, M. Zhan, J.C. Chang, M.S. Wicha, Breast cancer stem cells transition between epithelial and mesenchymal states reflective of their normal counterparts, Stem Cell Rep. 2 (2014) 78–91.
[97] A. De Luca, M. Fiorillo, M. Peiris-Pages, B. Ozsvari, D.L. Smith, R. Sanchez-Alvarez, U.E. Martinez-Outschoorn, A.R. Cappello, V. Pezzi, M.P. Lisanti, F. Sotgia, Mitochondrial biogenesis is required for the anchorage-independent survival and propagation of stem-like cancer cells, Oncotarget 6 (2015) 14777–14795.
[98] C. Morata-Tarifa, G. Jimenez, M.A. Garcia, J.M. Entrena, C. Grinan-Lison, M. Aguilera, M. Picon-Ruiz, J.A. Marchal, Low adherent cancer cell subpopulations are enriched in tumorigenic and metastatic epithelial-to-mesenchymal transition-induced cancer stem-like cells, Sci. Rep. 6 (2016) 18772.
[99] F. Pantano, M. Croset, K. Driouch, N. Bednarz-Knoll, M. Iuliani, G. Ribelli, E. Bonnelye, H. Wikman, S. Geraci, F. Bonin, S. Simonetti, B. Vincenzi, S.S. Hong, S. Sousa, K. Pantel, G. Tonini, D. Santini, P. Clezardin, Integrin alpha5 in human breast cancer is a mediator of bone metastasis and a therapeutic target for the treatment of osteolytic lesions, Oncogene 40 (2021) 1284–1299.
[100] P.H. Krebsbach, L.G. Villa-Diaz, The role of Integrin alpha6 (CD49f) in stem cells: more than a conserved biomarker, Stem Cells Dev 26 (2017) 1090–1099.
[101] R.L. Stewart, K.L. O'Connor, Clinical significance of the integrin alpha6beta4 in human malignancies, Lab. Invest. 95 (2015) 976–986.
[102] T. Brabletz, A. Jung, S. Spaderna, F. Hlubek, T. Kirchner, Opinion: migrating cancer stem cells - an integrated concept of malignant tumour progression, Nat. Rev. Cancer 5 (2005) 744–749.
[103] T. Shibue, R.A. Weinberg, EMT, CSCs, and drug resistance: the mechanistic link and clinical implications, Nat. Rev. Clin. Oncol. 14 (2017) 611–629.
[104] E.R. Nelson, The significance of cholesterol and its metabolite, 27-hydroxycholesterol in breast cancer, Mol. Cell. Endocrinol. (2017).
[105] W.H. Matsui, Cancer stem cell signaling pathways, Medicine (Baltim.) 95 (2016) S8–S19.
[106] W. Xue, L. Yang, C. Chen, M. Ashrafizadeh, Y. Tian, R. Sun, Wnt/beta-catenin-driven EMT regulation in human cancers, Cell. Mol. Life Sci. 81 (2024) 79.
[107] N.M. Ghahhari, S. Babashah, Interplay between microRNAs and WNT/beta-catenin signalling pathway regulates epithelial-mesenchymal transition in cancer, Eur. J. Cancer 51 (2015) 1638–1649.
[108] S. Shang, F. Hua, Z.W. Hu, The regulation of beta-catenin activity and function in cancer: therapeutic opportunities, Oncotarget 8 (2017) 33972–33989.
[109] F. Yu, C. Yu, F. Li, Y. Zuo, Y. Wang, L. Yao, C. Wu, C. Wang, L. Ye, Wnt/beta-catenin signaling in cancers and targeted therapies, Signal Transduct. Targeted Ther. 6 (2021) 307.
[110] C.M. Quinn, W. Jessup, J. Wong, L. Kritharides, A.J. Brown, Expression and regulation of sterol 27-hydroxylase (CYP27A1) in human macrophages: a role for RXR and PPARgamma ligands, Biochem. J. 385 (2005) 823–830.
[111] L. Yu, L. Xu, H. Chu, J. Peng, A. Sacharidou, H.H. Hsieh, A. Weinstock, S. Khan, L. Ma, J.G.B. Duran, J. McDonald, E.R. Nelson, S. Park, D.P. McDonnell, K. J. Moore, L.J. Huang, E.A. Fisher, C. Mineo, L. Huang, P.W. Shaul, Macrophage-to-endothelial cell crosstalk by the cholesterol metabolite 27HC promotes atherosclerosis in male mice, Nat. Commun. 14 (2023) 4101.
[112] K. O'Brien, K. Breyne, S. Ughetto, L.C. Laurent, X.O. Breakefield, RNA delivery by extracellular vesicles in mammalian cells and its applications, Nat. Rev. Mol. Cell Biol. 21 (2020) 585–606.
[113] N.A. Skrypina, A.V. Timofeeva, G.L. Khaspekov, L.P. Savochkina, R. Beabealashvilli, Total RNA suitable for molecular biology analysis, J. Biotechnol. 105 (2003) 1–9.
[114] H. Schwarzenbach, Clinical relevance of circulating, cell-free and exosomal microRNAs in plasma and serum of breast cancer patients, Oncol. Res. Treat. 40 (2017) 423–429.
[115] B.R. Pires, D.E.A. Is, L.D. Souza, J.A. Rodrigues, A.L. Mencalha, Targeting cellular signaling pathways in breast cancer stem cells and its implication for cancer treatment, Anticancer Res. 36 (2016) 5681–5691.
[116] W.W. Tong, G.H. Tong, Y. Liu, Cancer stem cells and hypoxia-inducible factors (Review), Int. J. Oncol. 53 (2) (2018 Aug) 469–476, https://doi.org/10.3892/ijo.2018.4417. Epub 2018 May 22. PMID: 29845228.
[117] E.N. Nolte-'t Hoen, H.P. Buermans, M. Waasdorp, W. Stoorvogel, M.H. Wauben, P.A. t Hoen, Deep sequencing of RNA from immune cell-derived vesicles uncovers the selective incorporation of small non-coding RNA biotypes with potential regulatory functions, Nucleic Acids Res. 40 (2012) 9272–9285.
[118] D. Koppers-Lalic, M. Hackenberg, I.V. Bijnsdorp, M.A.J. van Eijndhoven, P. Sadek, D. Sie, N. Zini, J.M. Middeldorp, B. Ylstra, R.X. de Menezes, T. Wurdinger, G. A. Meijer, D.M. Pegtel, Nontemplated nucleotide additions distinguish the small RNA composition in cells from exosomes, Cell Rep. 8 (2014) 1649–1658.
[119] M.L. Squadrito, C. Baer, F. Burdet, C. Maderna, G.D. Gilfillan, R. Lyle, M. Ibberson, M. De Palma, Endogenous RNAs modulate microRNA sorting to exosomes and transfer to acceptor cells, Cell Rep. 8 (2014) 1432–1446.
[120] G. He, J. Liu, Y. Yu, S. Wei, X. Peng, L. Yang, H. Li, Revisiting the advances and challenges in the clinical applications of extracellular vesicles in cancer, Cancer letters 593 (2024) 216960.
[121] L. Qian, P. Chen, S. Zhang, Z. Wang, Y. Guo, V. Koutouratsas, J.S. Fleishman, C. Huang, S. Zhang, The uptake of extracellular vesicles: research progress in cancer drug resistance and beyond, Drug Resist. Updates 79 (2025) 101209.
[122] Y. Zou, H. Zhang, P. Chen, J. Tang, S. Yang, C. Nicot, Z. Guan, X. Li, H. Tang, Clinical approaches to overcome PARP inhibitor resistance, Mol. Cancer 24 (2025) 156.
[123] J. Shi, Y. Shen, J. Zhang, Emerging roles of small extracellular vesicles in metabolic reprogramming and drug resistance in cancers, Cancer Drug Resist 7 (2024) 38.
[124] Y. Takeuchi, T. Tanegashima, E. Sato, T. Irie, A. Sai, K. Itahashi, S. Kumagai, Y. Tada, Y. Togashi, S. Koyama, E.A. Akbay, T. Karasaki, K. Kataoka, S. Funaki, Y. Shintani, I. Nagatomo, H. Kida, G. Ishii, T. Miyoshi, K. Aokage, K. Kakimi, S. Ogawa, M. Okumura, M. Eto, A. Kumanogoh, M. Tsuboi, H. Nishikawa, Highly immunogenic cancer cells require activation of the WNT pathway for immunological escape, Sci Immunol 6 (2021) eabc6424.
[125] P. Nallasamy, R.K. Nimmakayala, S. Parte, A.C. Are, S.K. Batra, M.P. Ponnusamy, Tumor microenvironment enriches the stemness features: the architectural event of therapy resistance and metastasis, Mol. Cancer 21 (2022) 225.
[126] X. Xu, M. Zhang, F. Xu, S. Jiang, Wnt signaling in breast cancer: biological mechanisms, challenges and opportunities, Mol. Cancer 19 (2020) 165.
[127] C. Samant, R. Kale, K.S.R. Pai, K. Nandakumar, M. Bhonde, Role of Wnt/beta-catenin pathway in cancer drug resistance: insights into molecular aspects of major solid tumors, Biochem. Biophys. Res. Commun. 729 (2024) 150348.
[128] M. Kahn, Can we safely target the WNT pathway? Nat. Rev. Drug Discov. 13 (2014) 513–532.

[129] A. Sharma, J. Zalejski, S.V. Bendre, S. Kavrokova, H.S. Hasdemir, D.G. Ozgulbas, J. Sun, K.C. Pathmasiri, R. Shi, A. Aloulou, K. Berkley, C.F. Delisle, Y. Wang, E. Weisser, P. Buweneka, D. Pierre-Jacques, S. Mukherjee, D.A. Abbasi, D. Lee, B. Wang, V. Gevorgyan, S.M. Cologna, E. Tajkhorshid, E.R. Nelson, W. Cho, Cholesterol-targeting wnt-beta-catenin signaling inhibitors for colorectal cancer, Nat. Chem. Biol. (2025).
[130] G.L. Burn, A. Foti, G. Marsman, D.F. Patel, A. Zychlinsky, The neutrophil, Immunity 54 (2021) 1377–1391.
[131] V. Papayannopoulos, Neutrophil extracellular traps in immunity and disease, Nat. Rev. Immunol. 18 (2018) 134–147.
[132] J. Park, R.W. Wysocki, Z. Amoozgar, L. Maiorino, M.R. Fein, J. Jorns, A.F. Schott, Y. Kinugasa-Katayama, Y. Lee, N.H. Won, E.S. Nakasone, S.A. Hearn, V. Kuttner, J. Qiu, A.S. Almeida, N. Perurena, K. Kessenbrock, M.S. Goldberg, M. Egeblad, Cancer cells induce metastasis-supporting neutrophil extracellular DNA traps, Sci. Transl. Med. 8 (2016) 361ra138.
[133] J.M. De Cock, T. Shibue, A. Dongre, Z. Keckesova, F. Reinhardt, R.A. Weinberg, Inflammation triggers Zeb1-Dependent escape from tumor latency, Cancer Res. 76 (2016) 6778–6784.
[134] X.Y. He, Y. Gao, D. Ng, E. Michalopoulou, S. George, J.M. Adrover, L. Sun, J. Albrengues, J. Dassler-Plenker, X. Han, L. Wan, X.S. Wu, L.S. Shui, Y.H. Huang, B. Liu, C. Su, D.L. Spector, C.R. Vakoc, L. Van Aelst, M. Egeblad, Chronic stress increases metastasis via neutrophil-mediated changes to the microenvironment, Cancer Cell 42 (2024) 474–486 e412.